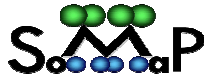




JOHANNES KEPLER
UNIVERSITÄT LINZ | JKU



Department of
Soft Matter Physics

Dielectric Elastomer Transducers

Christoph Keplinger

Linz, April 2010

Research visit from September 1st, 2009 to February 28th, 2010

to Harvard University, Cambridge, Massachusetts, USA

Supervisors:

Professor Siegfried Bauer, JKU, Austria

Professor Zhigang Suo, HARVARD, USA

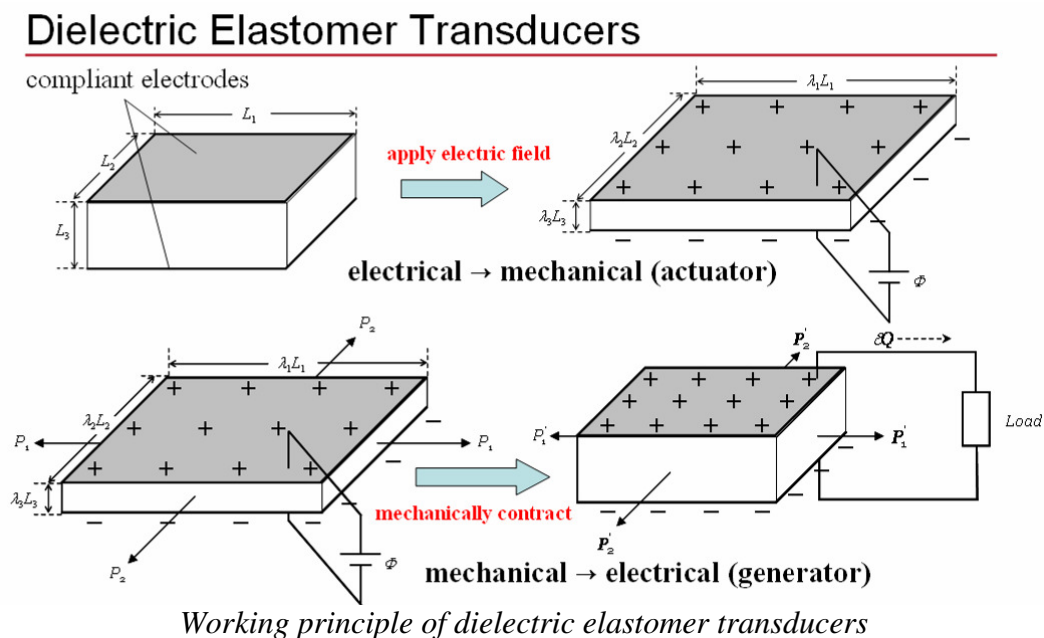


Contents

Preface	04
Scientific paper	06
Appendix 1	41
Appendix 2	62
Confirmation Professor Suo	76
Confirmation Professor Bauer	77

Preface

Dielectric elastomer transducers consist of elastomer membranes sandwiched between compliant electrodes and can be considered as soft deformable capacitors. When voltage is applied, the membrane thins down and expands in its area. As such, dielectric elastomers are commonly used as actuators. On the other hand, a reduction of tensile force on a pre-stretched and pre-charged dielectric elastomer membrane under open circuit conditions increases voltage, allowing electric charges to be boosted from a low voltage source to a high voltage reservoir. In this case, dielectric elastomers are used as generators:



As stated in the research proposal, the main focus of my research visit to Harvard University should be on the modeling of electrode-free charge controlled actuators. The primary research paper about this work was already sent for review at the time the research visit in the USA should start. The second part of the research on electrode-free actuators was planned to start after the final publication of the first paper. Due to the copious reviewing and revision time in the renowned PNAS, the journal of the National Academy of Sciences of the United States of America, the paper was not published until March 2010. (open access publication; displayed in Appendix 2)

The refocusing of my research assignment was not difficult, as the group around Professor Zhigang Suo started to work on dielectric elastomer generators, the second branch of possible applications of dielectric elastomer transducers, besides actuator applications. The results of this collaboration on *“Dielectric Elastomer Generators: How much energy can be converted?”* shall be the main part of this research report. The paper is planned to be published in a focused section on “Electroactive Polymer Mechatronics” of the “IEEE/ASME TRANSACTIONS ON MECHATRONICS” (Paper submission April 1, 2010; final publication after peer review process: February 2011; the “Scientific paper” part of this research report is subject to copyright conditions of IEEE/ASME and should not be published elsewhere). In the “Acknowledgement” section of this paper the Austrian Marshall Plan Foundation is mentioned: *“...Additionally the work was supported by the Austrian Science Fund and by the Austrian Marshall Plan Foundation, through the sponsoring of a half-year visit of C Keplinger to Harvard University...”*

The work on dielectric elastomer generators was additionally presented at the 2010 MRS spring meeting (April 5-9, 2010) of the Materials Research Society in San Francisco, California, USA. The talk on the *“Aptitude of Dielectric Elastomer Transducers for Energy Harvesting Generators”* combined our theoretical findings about dielectric elastomer generators with recent findings from an experiment in our JKU Linz laboratory. The PowerPoint slides of the oral presentation are displayed in Appendix 1. The logo of the Austrian Marshall Plan Foundation was presented in the title slide.

Finally, I want to thank the Austrian Marshall Plan Foundation for sponsoring my six month research visit to Harvard University. In compliance with the spirit of the Marshall Plan, I was able to strengthen the fruitful collaboration between the US group around Professor Zhigang Suo and the Austrian group around Professor Siegfried Bauer. The publication of the first joint scientific paper is in process.

Scientific paper

Dielectric Elastomer Generators: How much energy can be converted?

Soo Jin Adrian Koh^{1,3}, Christoph Keplinger^{1,2}, Tiefeng Li^{1,4}, Siegfried Bauer^{2,a}, Zhigang Suo^{1,b}

¹*School of Engineering and Applied Sciences, Harvard University
Cambridge, Massachusetts 02138, USA*

²*Soft-Matter Physics, Johannes Kepler University
Altenbergerstrasse 69, A-4040 Linz, Austria*

³*Institute of High Performance Computing
1 Fusionopolis Way, #16-16 Connexis, Singapore 138632, Singapore*

⁴*Institute of Applied Mechanics, Zhejiang University,
38 Zheda Road, Hangzhou, Zhejiang 310027, China*

Abstract

Dielectric elastomer can serve as generators to convert mechanical energy into electrical energy. While energy of conversion between 0.1 mJ/g and 400 mJ/g have been reported, it is not known if these figures are limited by fundamental principles, or if there is room for improvement. One may even wish to select and design materials specifically for dielectric elastomer generators but currently, such efforts are largely made by performing experiments. This paper develops a theoretical approach that plots limit states on work-conjugate *operation maps*, and computes the maximum energy of conversion. The limit states are defined by well-established mechanisms of failure. The effect of varying material parameters on the energy of conversion is studied. Simple formulas are proposed to guide the selection and design of elastomers for generators. It is found that natural rubber outperforms VHB elastomer as a generator at strains less than 15%. Furthermore, a moderately stiff elastomer can convert energy at 1.0 J/g by using a strain of operation of 100%.

^aemail: Siegfried.Bauer@jku.at

^bemail: suo@seas.harvard.edu

1. Introduction

A dielectric elastomer transducer consists of an elastomer membrane sandwiched between compliant electrodes, and can be considered as a deformable capacitor [1,2]. When a voltage is applied, the membrane thins down and expands in its area. The elastomer is commonly used as an actuator, converting electrical energy into mechanical energy [2–8]. On the other hand, for a pre-stretched and pre-charged membrane under open circuit conditions, a reduction of tensile force thickens the membrane and increases the voltage, boosting electric charges from a low-voltage source to a high-voltage reservoir. In this case, the elastomer is used as a generator, converting mechanical energy to electrical energy [9,10].

Dielectric elastomer generators (DEGs) are promising for small-scale energy harvesting [11–13], as well as for large-scale energy generation [11]. They are ideally suited to harvest the vast and concentrated amount of energy stored in ocean waves due to impedance match, low cost, and reliability. Elastomers are at least 7 times lighter than piezoceramics and ferromagnets. They are highly stretchable, which enables excellent force-coupling. Research has shown that the electromechanical conversion efficiency is high [14]. Being a polymer material, dielectric elastomers do not rust under the corrosive action of ocean sprays. Finally, elastomer materials like natural vulcanized rubber and polyacrylate VHB 3M™ elastomers are widely available and low in cost. All these advantages may translate to efficient generators that are light-weight, cost-efficient, reliable and low in maintenance.

While dielectric elastomer actuators (DEAs) are extensively studied, research on its counterpart as a generator is sparse. A limited number of experiments were conducted on dielectric elastomer generators [9,11–13], with strain of operation often restricted to less than 100%. It is well-known that typical elastomers exhibit strains in excess of 500% [2,15–19]. In one particular experiment, a very high energy of conversion of 0.4 J/g has been given, without specification of the experimental conditions, preventing the repetition of the experiment. Nevertheless, the experiment shows the large potential of dielectric elastomer generators, possibly exceeding energy of conversion of piezoceramics and electrostrictive polymers by an order of magnitude [20–22]. Even under moderate strain conditions, preferable when reliability is a concern, elastomer generators may potentially be very attractive alternatives to

piezoceramics and electrostrictive polymers. It will be interesting, therefore, to investigate how dielectric elastomer generators perform in the whole strain region, from low strains preferable for long time, reliable operation to high strains, outlining the full potential and also the limits of the technique. Material models that capture the full range of elastomer stress-strain behavior [15,16], including strain-stiffening at high stretches where the polymer chains approach their extension limit, will enable us to determine the potential of the technology from low strain to high strain and to determine the limits for the energy of conversion.

Based on a previous study [10], we present a theoretical framework to define the safe operation regime for a given dielectric elastomer. This framework is based on the consideration of limit states that will lead to irrecoverable failure of the elastomer. These limit states are defined as a set of four well-known failure mechanisms for dielectric elastomer membranes – electrical breakdown, electromechanical instability (or pull-in instability), loss of tension and material rupture [10,18,23,24]. While the mechanisms for electromechanical instability, loss of tension and material rupture are well-understood [18,24,25], the mechanisms leading to electrical breakdown are complex, and remain poorly-understood. In our analysis, we shall assume that the dielectric elastomer undergoes breakdown when the true electric field attains a critical magnitude E_{EB} , known as the dielectric strength. It has been shown experimentally that E_{EB} can significantly dependent on stretch for VHB elastomers [17,18]. Imagine that one is able to operate dielectric elastomer generators along these limit states, the amount of energy that can be converted is at the theoretical maximum. These limit states are plotted on work conjugate force-displacement, and voltage-charge planes, which enable fast and easy computation of the energy of conversion. This framework will not be limited to specific material models, therefore more detailed models can be used at any time when it is necessary to consider specific aspects not covered by the models used at the present stage. New experimental findings can also be incorporated.

We shall first use our model to compare the energy conversion performance between the commonly used VHB elastomer and natural rubber. All the necessary mechanical material properties are obtained from fitting experimental stress-strain curves with the Arruda-Boyce model [16], which is based on the statistical physics of macromolecules, including the strain-

stiffening part in the vicinity of the polymer chain extension limit. The maximum possible stretch for the elastomer is therefore determined by the extension limit of polymer chains. The electrical properties are taken from experimental results for VHB elastomer, where the dielectric strength is fitted to a phenomenological model, incorporating the fact that the dielectric strength is enhanced by stretching. The energy conversion performance for the entire range of operational stretch, from very small strains ($\approx 1\%$) up to the maximum possible stretch at the extension limit, was compared for both materials. Between strains of operation of 1% and 500%, we found that the maximum energy of conversion spans at least two orders of magnitude.

Following this, a study on the effect of varying characteristic mechanical and electrical material parameters on the energy of conversion is conducted. We select the characteristic stiffness μ and the Maxwell stress at electrical breakdown ϵE_{EB}^2 as the material parameters to be varied. A linear model for small strain operation and a general non-linear model for large stretch operation are used to establish equations that predict the maximum energy of conversion. These equations allow quick and reasonably accurate estimations of the maximum energy of conversion once the relevant material parameters are known, which could aid in the selection and design of new dielectric elastomer generator materials.

2. Limit State Analysis for a Dielectric Elastomer

Consider a dielectric elastomer sandwiched between two compliant electrodes as shown in Fig. 1a. Subject to a voltage through its thickness and mechanical loading in the planar directions, a dielectric elastomer thins down and expands in area (Fig. 1b). A prior study has shown that equal-biaxial stretching converts more energy at a lower input voltage as compared to uniaxial stretching [26], as such; we shall adopt this mode of stretching in our analysis. Assuming incompressibility, Fig. 1 shows the dimensions of a dielectric elastomer subject to equal-biaxial load at the reference (Fig. 1a) and the activated states (Fig. 1b). It is assumed that the elastomer is a hyperelastic material, and can be satisfactorily described by a free-energy function $W(\lambda)$, with its stress given by the equations-of-state. Dissipative effects like

viscoelasticity and dielectric relaxation are ignored in our analysis. In this section, we propose a limit state model to compute the maximum energy of conversion for a dielectric elastomer.

Subject to the mechanical and electrical load configuration as shown in Fig. 1b, the equation-of-state for the elastomer at the activated state is given as: $\sigma - \sigma_3 = (\lambda/2)(\partial W/\partial \lambda) = G(\lambda)$, where σ is the equal-biaxial true stress in each planar direction, σ_3 is the true stress in the thickness direction and $G(\lambda)$ is the stress-strain relationship for the elastomer. Assuming liquid-like dielectric response and ignoring the effects of dielectric relaxation, the voltage applies an equivalent compressive mechanical stress in the thickness direction, known as the Maxwell stress [1,27]. Adopting the expression of Maxwell stress given in [27], the following force-balance and capacitive relations can be written:

$$\frac{P}{LH} + \varepsilon \left(\frac{\Phi}{H} \right)^2 \lambda^3 = F(\lambda) \quad (1a)$$

$$\frac{Q}{L^2} = \varepsilon \left(\frac{\Phi}{H} \right) \lambda^4 \quad (1b)$$

where P , λ and Φ are mechanical force, stretch and voltage respectively, as defined in Fig. 1, Q is the magnitude of charge on each electrode due to Φ , ε is the dielectric permittivity and $\varepsilon = \varepsilon_r \varepsilon_0$, where ε_r is the dielectric constant and ε_0 is the dielectric permittivity of vacuum. $F(\lambda)$ is the nominal stress-strain relationship, and $\lambda F(\lambda) = G(\lambda)$. There are four field variables in equation (1): P, λ, Φ, Q . One may choose to prescribe any two of the four field variables and, assuming that $F(\lambda)$ is known, solve the other two variables using equation (1). Equation (1) therefore completely describes the electromechanical response of a dielectric elastomer transducer.

There are numerical limits whereby the four field variables can take. These limits are either prescribed by the user, or determined by the failure modes of the dielectric elastomer. Well-known failure modes include electrical breakdown, electromechanical instability, loss of tension and material rupture [10,18,23,24]. These failure modes define operational limit states for the dielectric elastomer. By plotting these limit states on work-conjugate planes of P - λ and Φ - Q , the energy of conversion per cycle of operation can be computed by an area enclosed by a

prescribed cycle on each plane. The limit states define the boundaries of operation. These plots are termed the *operation maps* of a dielectric elastomer.

When the elastomer is highly-stretched, the polymer chains could uncoil to a point where further stretch is not possible without undergoing material failure. One may also choose to limit the range of operation to modest stretches, in order to improve durability and reliability of operation. Define the maximum stretch as λ_{\max} , putting $\lambda = \lambda_{\max}$ in equation (1), we have:

$$\lambda = \lambda_{\max}, \quad \frac{\Phi}{H} = \frac{\lambda_{\max}^{-4}}{\varepsilon} \left(\frac{Q}{L^2} \right) \quad (2)$$

Under an exceptionally high electric field, the elastomer will experience electrical breakdown (*EB*) [17,21,22]. The electric field that causes breakdown is known as the dielectric strength. Under an experimental setting, the voltage that causes *EB* may be sensitive to material imperfections like voids, inclusions or material inhomogeneities [28]. Experiments have shown that the observed dielectric strength of polymers may be dependent on various physical properties like stretch [17,18], small strain thickness [29] and material stiffness [30]. Define the maximum electric field the elastomer can take before undergoing *EB* as E_{EB} , putting into (1):

$$\frac{P}{LH} = F(\lambda) - \varepsilon \lambda^{-1} E_{EB}^2, \quad \frac{\Phi}{H} = \varepsilon \left(\frac{Q}{L^2} \right)^{-1} E_{EB}^2 \quad (3)$$

Experiments can be conducted to determine the dielectric strength, and its dependence on various physical properties. An analytical expression can be selected and optimally-fitted to the experimental data.

As the voltage is increased, the elastomer reduces in thickness, so that the positive feedback between a thinner elastomer and a higher true electric field may result in electromechanical instability (*EMI*) [23,25,31]. However, it should also be noted that, due to strain-stiffening of the polymer at large deformation, *EMI* can be eliminated by prestressing the elastomer [32]. Mathematical equations for *EMI* to occur have been established previously [25], and shall not be repeated here. Differentiating the intensive variables P and Φ , with respect to the extensive variables λ and Q , we have:

$$\left(\frac{1}{LH}\right)\frac{\partial P}{\partial\lambda} + \left[2\lambda\Phi\varepsilon\left(\frac{\lambda}{H}\right)^2\right]\frac{\partial\Phi}{\partial\lambda} = \frac{\partial F}{\partial\lambda} - 3\lambda^2\varepsilon\left(\frac{\Phi}{H}\right)^2 \quad (4a)$$

$$\left(\frac{1}{L^2}\right)\frac{\partial\Phi}{\partial\lambda} = \varepsilon\left[\left(\frac{\lambda^4}{H}\right)\frac{\partial\Phi}{\partial\lambda} + \left(\frac{\Phi}{H}\right)4\lambda^3\right]\frac{\partial\Phi}{\partial Q} \quad (4b)$$

At *EMI*, we have: $\partial\Phi/\partial\lambda = 0$, and from (4b): $\partial\Phi/\partial Q = 0$. For a fixed P : $\partial P/\partial\lambda = 0$. From (4a) and (1), we have:

$$\frac{P}{LH} = F(\lambda) - \frac{\lambda}{3}\frac{\partial F}{\partial\lambda}, \quad \frac{\Phi}{H} = \left[\varepsilon\left(\frac{Q}{L^2}\right)\right]^{-1/3}\left(\frac{1}{3}\frac{\partial F}{\partial\lambda}\right)^{2/3} \quad (5)$$

where λ in the Φ - Q expression can be replaced by Q using (1b).

For a dielectric elastomer membrane, it is desirable to keep the membrane in tension, as any compressive stress in the planar directions will lead to the formation of wrinkles, which may cause premature failure. This limiting condition (*LT*) is given as:

$$\frac{P}{LH} = 0, \quad \frac{\Phi}{H} = \frac{1}{\varepsilon}\left(\frac{Q}{L^2}\right)^{-3/5}\left[F(\lambda)\right]^{4/5} \quad (6)$$

where λ in the Φ - Q expression can be replaced by Q using (1b).

Finally, it should be noted that the fundamental thermodynamic stability condition: $\sigma \leq (\lambda/2)(\partial W/\partial\lambda)$ must always be obeyed. The thermodynamic stability limit is given by the nominal stress-strain relationship:

$$\frac{P}{LH} = F(\lambda) \quad \text{at} \quad \frac{\Phi}{H} = \frac{Q}{L^2} = 0 \quad (7)$$

The stress-strain relationship can be obtained experimentally, and an analytical function $F(\lambda)$ can be selected and optimally-fitted to the experimental data.

Equations (2), (3), (5)–(7) collectively define the limit states which the dielectric elastomer electromechanical transducer can operate in the P - λ and the Φ - Q planes. Operating along these limit states gives an energy conversion cycle that gives the maximum electromechanical energy of conversion.

3. Material Models

For a given dielectric elastomer, the stress-strain relationship, and the observed dielectric strength can be obtained experimentally [15–18]. EMI and LT are analytically obtained from equations (5) and (6). λ_{\max} can either be prescribed, or simply allow the material to stretch up to the rupture stretch. Therefore, to have a complete analytical representation of the limit states, suitable material models for $F(\lambda)$ and E_{EB} in equations (7) and (3) must be established.

A key objective of this work is to study the effect of basic hyperelastic material properties like small strain shear modulus μ , λ_{\max} and electrical properties like dielectric constant ϵ_r and dielectric strength E_{EB} has on the maximum energy of conversion of a dielectric elastomer generator. To that end, we have selected a model for $F(\lambda)$ that describes the hyperelastic behavior based on the macromolecular network structure of the elastomer. The entire range of stretch, including the strain-stiffening at high stretches is covered by the chosen model. This enables us to at least have a qualitative insight to the stress levels required if one desires to operate at high stretches, and also to study the significance of the stiffening part on the energy conversion of a dielectric elastomer generator.

The Arruda-Boyce model [16] describes the molecular structure of a rubber-like material with eight chains oriented in space, where the deformation behavior of each individual chain is defined by Langevin chain statistics [33]. For the statistical mechanics description, a single chain is defined as the part of a polymer chain between two successive chemical crosslinks. This chain part is modeled as a chain of n freely-jointed, rigid, statistical links of equal length, the so called “Kuhn length”. This length spans over a specific number of chemical bonds along the polymer chain, depending on the material specific properties of these chemical bonds, like rotation angle around single bonds and the ratio between double and single bonds. In any case the Kuhn length has to be long enough to justify the assumption of freely-jointed links.

The free-energy density of the elastomer is given as [15,16,33]:

$$W = NkTn \left(\frac{\zeta}{\tanh \zeta} - 1 + \log \frac{\zeta}{\sinh \zeta} \right) \quad (8)$$

where kT is the temperature in the unit of energy, ζ is the normalized force in each chain, and N is the number of chains per unit volume. N is also proportional to the number of chemical crosslinks. Based on Kuhn's Langevin statistics [33], the stretch on each polymer chain Λ is related to the normalized force ζ as:

$$\Lambda = \sqrt{n} \left(\frac{1}{\tanh \zeta} - \frac{1}{\zeta} \right) \quad (9)$$

where n is the number of statistical links in the chain. For an elastomer subject to principal stretches λ_1 , λ_2 and λ_3 , Arruda and Boyce [16] proposed that:

$$\Lambda = \sqrt{\frac{\lambda_1^2 + \lambda_2^2 + \lambda_3^2}{3}} \quad (10a)$$

In the limit $\zeta \rightarrow 0$ the neo-Hookean model is recovered, with the small strain shear modulus $\mu = NkT$.

For an incompressible elastomer subject to equal-biaxial stretch, equation (10a) becomes:

$$\Lambda = \sqrt{\frac{2\lambda^2 + \lambda^{-4}}{3}} \quad (10b)$$

Based on the random-walk statistics [15,16,33], the polymer chain attains its fully-stretched length when $\Lambda = \sqrt{n}$. From (10b), this imposes a limit stretch (λ_{lim}) by which the elastomer can deform, given as:

$$2\lambda_{\text{lim}}^2 + \lambda_{\text{lim}}^{-4} = 3n \quad (11)$$

From equation (9), it could be seen that when $\Lambda \rightarrow \sqrt{n}$, $\zeta \rightarrow \infty$. Hence, given n , the maximum possible stretch can be solved from equation (11).

Equations (8)–(10) define a free-energy function $W(\lambda)$ for an elastomer subject to equal-biaxial stretch. Experiments often measure the nominal stress (P/LH), instead of the true stress ($P\lambda/LH$) to plot the stress-strain data [15–18]. Following this, we define the nominal stress-strain relation $F(\lambda)$, given by the equation-of-state: $F(\lambda) = (1/2)(\partial W/\partial \lambda)$. From (8)–(10), we have:

$$F(\lambda) = \mu \zeta \sqrt{n} \frac{\lambda - \lambda^{-5}}{3\Lambda} \quad (12)$$

Equation (12) establishes an analytical function for $F(\lambda)$ in equations (1a) and (5)–(7).

From (12), the shape of the stress-strain relationship is governed by the number of statistical links n in each chain, and the small strain shear modulus μ . The latter is proportional to the density of chemical crosslinks N , and the ambient temperature T . Fig. 2 shows the effects n and μ have on the stress-strain behavior of an elastomer. In general, n controls the limit stretch and μ controls the amount of load required to deform the elastomer to a specific stretch. Fig. 3a shows the values for n and μ when the material model was optimally-fitted to experimental data of natural rubber (NR) [15,16], and VHB acrylic elastomers (VHB) [18]. Two observations can be made from Fig. 3a. First, the material properties n and μ are not significantly different when fitted to uniaxial and equal-biaxial data for NR. Second, the maximum stretches for both VHB and NR under uniaxial stretch are similar, while the small strain shear stiffness for VHB is about half-order magnitude smaller than NR. The first observation allows us to transplant uniaxial stretch data for use in an equal-biaxial stretch configuration, and make good qualitative conclusions on the equal-biaxial stress-strain behavior. The second observation allows us to understand the energy conversion performance between a soft elastomer (VHB) and a stiff elastomer (NR).

For an elastomer with a specific thickness, the dielectric elastomer experiences electrical breakdown when its dielectric strength (E_{EB}) is reached. We may write: $E_{EB} = \Phi_{EB} / h$. E_{EB} is usually expressed as a constant, and h is the thickness at breakdown. But experimental data on VHB dielectric elastomer shows that E_{EB} may be dependent on stretch [17,18]. The experimental data are fit to:

$$E_{EB}(\lambda) = [E_{EB}(\lambda = 1)] \lambda^R \quad (13)$$

where $E_{EB}(\lambda = 1)$ is the electric field required to cause electrical breakdown when the stretch is fixed at $\lambda = 1.0$, and R is the degree of sensitivity of dielectric strength towards stretch. $R = 0$ implies that the dielectric strength is independent of stretch. Equation (13) establishes an analytical function for equation (3). Fig. 3b shows the values for $E_{EB}(\lambda = 1)$ and R when

equation (13) was optimally-fitted to experimental data for VHB elastomer with $H = 1.0$ mm [17,18]. The mechanism behind stretch-dependent dielectric strength is not well-understood. Hence, the model that we proposed here is phenomenological rather than physical.

Putting equations (11)–(13) into equations (2), (3), (5)–(7), we can now plot the limit states on work-conjugate P – λ and Φ – Q planes. The maximum energy of conversion for a dielectric elastomer can be computed from these plots.

In this section, we have described a simple formulation for the stress-strain relationship, based on the molecular picture of an elastomer, and the observed dielectric strength of a dielectric elastomer. This description allows useful information to be extracted for material scientists and engineers to understand how operational and material parameters affect the maximum energy of conversion. Theoretically-predicted mechanical material parameters for the single chain deformability n and the small strain shear modulus μ can be reproduced experimentally by clearly-defined concepts. The parameter n is influenced by the Kuhn length of specific polymer backbones and additionally by the average chain length, which itself is proportional to the density of chemical crosslinks. The parameter μ is proportional to the chain density and accordingly, the chemical crosslink density N , and the ambient temperature T . Consequently, under isothermal conditions, changing the crosslink density influences both the single chain deformability n and the small strain shear modulus μ . Nevertheless it is still possible to change n independently of μ by varying the stiffness of the polymer backbone what results in a variation of the Kuhn length. Furthermore, the addition of side chains, which are crosslinked to the polymer backbone but free on the other side, fills up the space in the polymer network, influencing the number of configuration states for single chains. Moreover elastomers of interpenetrating networks [34–38] may be considered for designing materials with desirable stress strain characteristics. In the subsequent sections, we shall compare the energy conversion performance of VHB and natural rubber as dielectric elastomer generators, and explore how different material parameters like μ , ε_r and E_{EB} affect the conversion performance.

4. Energy of Conversion for VHB and Natural Rubber

In this section, we select two distinct elastomers – VHB elastomer and natural rubber. We will use our model to compute the maximum energy of conversion for both materials as dielectric elastomer generators.

In the past decade, VHB elastomer has been extensively used in actuators and generators [2–13,38]. As a dielectric elastomer generator, it has been experimentally claimed that a VHB elastomer converts energy at a specific energy of 0.4 J/g, with the potential capability of harvesting energy at 1.0 J/g [9]. On the other hand, natural rubber is the most primitive form of elastomer, and it is abundant and cheap. No research was performed on natural rubber used as a generator.

Using existing experimental data for VHB elastomer under fast mechanical uniaxial loading (strain rate = 1.8 s⁻¹) [18], natural rubber under uniaxial and equal-biaxial loading [15,16], and the stretch-dependent dielectric strength of a 1.0mm thick VHB elastomer [17,18], we have determined the material parameters for equations (12) and (13), based on least-squares fitting (Fig. 3). The dielectric constants for VHB elastomer and natural rubber are $\epsilon_r = 4.5$ [39] and $\epsilon_r = 3.0$ [40], respectively, and are assumed to be insensitive to stretch. These fitted parameters were in excellent agreement with works performed by Plante [18] for VHB, and Arruda and Boyce [18] for natural rubber (NR). Due to the absence of experimental data for the stress-strain relationship for VHB under equal-biaxial loading, and the observed dielectric strength for NR, we have transplanted the material parameters from experimental data fits of uniaxial VHB stress-strain curves and used them for equal-biaxial stress-strain conditions. Also we used the observed dielectric strength of VHB for NR. Fig. 3a shows that the material parameters n and μ were not significantly different when fitted to both uniaxial and biaxial stretch data for NR, and that polymers in general have dielectric strengths between 10⁷ and 10⁸ V/m [38,40]. Therefore, we expect the transplanted parameters will not deviate significantly from an actual set of experimental data when it becomes available. Nevertheless, we have illustrated that equations (12) and (13) provided excellent fits to the existing experimental data

in Fig. 3. Any new set of experimental data available can be easily fitted with optimal parameters.

Under equal-biaxial loading, the limit states for VHB and NR were plotted in Fig. 4. In this figure, the dielectric elastomer generator was assumed to be stretched up to near limiting stretch in its operation. The shaded regions in Fig. 4 define the allowable states that the dielectric elastomer electromechanical transducer can operate without experiencing failure. By operating along the limit states, the theoretical maximum energy of conversion can be realized for the dielectric elastomer generator. As a generator, the cycle is described by a clockwise lap around the shaded region on the $P-\lambda$ plane, and an anti-clockwise lap around the shaded region on the $\Phi-Q$ plane. The theoretical limit for energy of conversion is given by the area bounded by the allowable states on the work-conjugate $P-\lambda$ plane, or the $\Phi-Q$ plane. For equal-biaxial stress, neglecting dissipative effects, the shaded area on the $\Phi-Q$ plane is two times of that in the $P-\lambda$ plane. For the VHB dielectric elastomer generator, the theoretical limit for maximum energy of conversion is 1.7 J/g (Fig. 4a), while that for NR is comparable, at 1.3 J/g (Fig. 4b). The voltage amplification when a pre-stretched and pre-charged elastomer is relaxed under the open-circuit condition is given by the height of the allowable region on the $\Phi-Q$ plane at various nominal charge densities (Q/L^2). When the elastomers are highly-stretched, it is possible to achieve a voltage amplification of more than 10 times when it is relaxed at a low charge condition. Voltage amplification reduces with increasing charge due to higher input voltage. This is because, with more charges on the electrodes, electrical breakdown will occur after a smaller amount of relaxation. There exists an optimal input voltage that maximizes the amount of energy that can be converted. One may design practical cycles within the allowable states, and determine the optimal level of input voltage that maximizes the energy of conversion. This has already been illustrated in a previous study [10], and shall not be repeated here.

To ensure long-term, reliable operation, one may wish to operate the dielectric elastomer generators at modest levels of stretch. Fig. 5a shows a schematic of how the shaded area is affected when λ_{\max} is reduced. It is well-known that piezoelectric transducers are able to convert energy at a maximum level of 1.0 mJ/g [20,21], subject to a strain of less than 1%.

Experiments have also been conducted on electrostrictive polymers, subject to strains of about 30%, and converting energy in the region of 10 mJ/g to 20 mJ/g [22]. Recent experiments conducted on dielectric elastomer generators were subject to maximum strains of about 100%, with claimed energy of conversion between 50 mJ/g and 400 mJ/g [9,11–13]. Fig. 5b and 5c shows the allowable states when the range of operation is limited to 5% and 30% for natural rubber. At the 5% range, both the stress-strain and voltage-charge response are approximately linear, and the energy conversion plots resemble that for a piezoelectric generator [20,21]. For the range of 30%, non-linearity shows up. Comparing Figs. 4b, 5b and 5c, we observed that the force P and the charge Q for small and large deformation differ by two or more orders of magnitude. As expected, the energy of conversion is 2.1 mJ/g and 16.8 mJ/g for 5% and 30% strain, respectively, which is two to three orders of magnitude smaller from the potential upper bound, when the dielectric elastomer generator is stretched up to its limit. In the case where the strain is 5%, the voltage amplification is small (< 50% boost). In the case where the strain is 30%, a voltage amplification up to two times is possible (> 100% boost).

Referring to Fig. 5a, by sweeping λ_{\max} line left-to-right on the P - λ plane, or rotating the same line about the origin of the Φ - Q plane, we may compute the maximum energy of conversion at various levels of operational stretch. Fig. 6 demonstrates the huge variability of energy conversion for a dielectric elastomer generator, spanning at least 2 orders of magnitude over the entire spectrum of operating stretch. In Fig. 6, we plot the curves for VHB and natural rubber (NR). Due to a lack of experimental data for the dielectric strength of NR versus stretch, NR with similar stretch-dependent dielectric strength as VHB (that is: $E_{EB} = 30 \text{ MV/m}$, $R = 1.13$), and NR with stretch-independent dielectric strength, where $E_{EB} = 30 \text{ MV/m}$, are plotted. For strains smaller than 15%, we can see that NR performs better in terms of energy conversion compared to VHB. For strains above 15%, the performance of NR is comparable to VHB if they exhibit similar stretch-dependent dielectric strengths. If the dielectric strength of NR is not improved by stretching, it performs poorer as compared to VHB. It appears that, in terms of energy conversion, NR outperforms VHB as a dielectric elastomer generator at small strains. At high stretches, the relative performance between them remains to be seen, as there

are currently no experimental data available on the dielectric strength of highly-stretched NR. To compare with existing technologies, to achieve comparable energy of conversion as piezoceramics, we need to operate NR at 3% and VHB at 5.5% strain. To achieve that displayed by electrostrictive polymers, strains between 20% and 30% are required. Exceeding the operational strain to values above 30% gives an improved figure of merit in comparison to piezoceramics and electrostrictive polymers. Reliability issues may favor elastomer generators, even when operated at low strains, being well adapted to be used in off-shore environments. Finally, it should also be noted that, although NR performs better than VHB at low strains, it is five times stiffer than VHB, which requires five times more force to stretch (Fig. 4).

5. Exploring Material Parameters on the Energy of Conversion

The previous section illustrated the energy of conversion for dielectric elastomer generators made from existing materials – VHB and natural rubber. We may then ask: What effect does material parameters have on the energy of conversion? What are the material parameters that we can look for in order to improve the amount of energy that can be converted? We shall explore some answers to these questions in this section.

We shall begin answering these questions by first considering a simple case where the operation is at small strain. In this case both the stress-strain and voltage-charge relations are linear (Fig. 5b). Referring to Fig. 5b, we may compute the energy of conversion by evaluating the shaded area on the P - λ plane. The shaded area is bounded by the stress-strain line, the EB line, the λ_{\max} line, and the LT line. Let e be the strain, where $e = \lambda - 1$, we may write an equation for the EB line on Fig. 5b as follows:

$$\frac{P}{LH} = \mu e - \varepsilon E_{EB}^2 \quad (14)$$

define e_{\max} as the maximum strain, we write the following equation for energy of conversion:

$$Y_{\max} = \varepsilon E_{EB}^2 \left(2e_{\max} - \frac{\varepsilon E_{EB}^2}{\mu} \right) \quad (15)$$

bearing in mind that the energy of conversion is two times the shaded area on the P - λ plane, and μ is the small strain shear modulus. One may immediately see, from equation (14), that if ϵE_{EB}^2 is too large, the internal stress of the dielectric elastomer will be compressive at EB . By limiting the dielectric elastomer generator to take only tensile stress, there exists an absolute maximum energy of conversion, given by: $Y_{\max} = \mu e_{\max}^2$. This situation occurs when the Maxwell stress at electrical breakdown (ϵE_{EB}^2) is so large that the material always loses tension before it undergoes electrical breakdown ($\epsilon E_{EB}^2 > \mu e_{\max}$). Hence, when the dielectric elastomer generator is operating within the linear range, two types of materials (Types A & B) can be identified. Type A is a dielectric elastomer with small ϵE_{EB}^2 such that $\epsilon E_{EB}^2 \leq \mu e_{\max}$. For the type A material, Y_{\max} increases linearly with e_{\max} , and saturates to $2\epsilon E_{EB}^2 e_{\max}$ at high μ . Type B is a dielectric elastomer with large ϵE_{EB}^2 such that $\epsilon E_{EB}^2 > \mu e_{\max}$. For this type of material, Y_{\max} increases linearly with μ , and quadratically with e_{\max} . It appears that, for operation in the small strain region, a stiff Type B elastomer is preferred.

For large deformation, we assume an arbitrary non-linear function $F(\lambda)$ that represents the nominal stress-strain curve. One form for $F(\lambda)$ was already given in equation (12). Assuming that the elastomer is sufficiently stiff so that EMI is averted at all levels of stretch (for instance Fig. 4b and Fig. 5c), we may write:

$$Y_{\max} = 2 \int_1^{\lambda_0} F(\lambda) d\lambda + 2 \int_{\lambda_0}^{\lambda_{\max}} \frac{F(\lambda) - P_{EB}(\lambda)}{LH} d\lambda \quad (16)$$

where λ_0 is the stretch whereby the EB or EMI line crosses the LT line on the P - λ plane, whichever is smaller. Physically, λ_0 is the critical stretch in a freely-expanding elastomer under an increasing voltage that corresponds to either the onset of EMI for a soft elastomer, or EB for a stiff elastomer. Based on previous studies, for a soft elastomer, EMI usually occurs in the vicinity of $\lambda_0 = 1.3$ [23,27]. Assuming that the elastomer undergoes irrecoverable breakdown when EMI occurs, this imposes a maximum for λ_0 at 1.3. Equation (12) suggests that $F(\lambda)$ may

take the following form: $F(\lambda) = \mu f(\lambda)$, where $f(\lambda)$ is the dimensionless nominal stress-strain curve. Substituting (3) and (13) into (16), we have:

$$\text{For } R = 0: \quad Y_{\max} = 2\mu \int_1^{\lambda_0} f(\lambda) d\lambda + 2\varepsilon E_{EB}^2 \log\left(\frac{\lambda_{\max}}{\lambda_0}\right) \quad (17a)$$

$$\text{For } R > 0: \quad Y_{\max} = 2\mu \int_1^{\lambda_0} f(\lambda) d\lambda + \varepsilon [E_{EB}(\lambda=1)]^2 \left(\frac{\lambda_{\max}^{2R} - \lambda_0^{2R}}{R} \right) \quad (17b)$$

For a soft elastomer such that *EMI* occurs over a specific range of stretch, the expression for Y_{\max} becomes very complex, and shall not be derived here. But as one may observe from Fig. 4a, *EMI* simply cuts out a portion of the shaded area otherwise bounded by the *EB* boundary in a soft elastomer. In this case, equation (17) will over-estimate Y_{\max} . For a very soft elastomer, *EMI* will cut out a significant portion of the shaded area. For such an elastomer, the full potential of its dielectric properties cannot be realized, as *EMI* always causes premature failure at low stretches. To obtain Y_{\max} for such elastomers, numerical methods must be used to compute the shaded area.

Assuming that $\lambda_{\max} \gg \lambda_0$, the first term on the right-hand-side becomes negligible. Equation (17) suggests that Y_{\max} again varies with εE_{EB}^2 . For an elastomer with its dielectric strength independent of stretch ($R = 0$), Y_{\max} increases with $\log(\lambda_{\max})$. For an elastomer with its dielectric strength that is enhanced by stretch ($R > 0$), Y_{\max} increases approximately with λ_{\max}^{2R}/R . In both cases, if the range of operation is in the high stretch region, the energy of conversion (Y_{\max}) depends on the Maxwell stress at electrical breakdown (εE_{EB}^2). Assuming that the mechanical stiffness (μ) is sufficient such that the elastomer always fail by *EB*, it will play little or no part in enhancing Y_{\max} . One may now conclude that εE_{EB}^2 plays a crucial part in determining Y_{\max} , in both the small strain and high stretch regions. We shall therefore explore the effects of varying μ and εE_{EB}^2 on Y_{\max} .

Fig. 7 shows the effect of varying small strain shear stiffness μ on the maximum energy of conversion Y_{\max} . In this plot, εE_{EB}^2 is assumed to be fixed, and do not vary with stretch. For the

smaller value of $\epsilon E_{EB}^2 = 0.024 \text{ MPa}$ (Fig. 7a), taken from the properties of natural rubber, Y_{\max} saturates at small strains of operation at high μ , and Y_{\max} can no longer be further increased beyond $\mu = 100 \text{ MPa}$ for the entire spectrum of strain of operation. Therefore, natural rubber appears to be at an optimal stiffness for energy conversion when operating at strains $> 100\%$. For small strain operation $< 100\%$, marginal gains in Y_{\max} can be achieved with a stiffer material. The expected theoretical maximum energy of conversion for natural rubber is therefore 100 mJ/g . So are there better candidates than natural rubber for energy conversion? Based on existing experimental data, the Maxwell stress at electrical breakdown for isoprene natural rubber was measured to be $\epsilon E_{EB}^2 = 0.11 \text{ MPa}$, and natural muscle gives $\epsilon E_{EB}^2 = 0.35 \text{ MPa}$ [38]. Hence, if ϵE_{EB}^2 can be increased to ten times that of natural rubber, that is: $\epsilon E_{EB}^2 = 0.24 \text{ MPa}$ (Fig. 7b), Y_{\max} is observed to increase about an order of magnitude if $\mu \geq 1.0 \text{ MPa}$. Y_{\max} remains relatively unchanged for the soft elastomer ($\mu = 0.05 \text{ MPa}$) at strain of operation $< 20\%$, as it now fails predominantly by *EMI* in that region, and therefore, the full dielectric potential cannot be realized. At higher strains of operation, due to strain-stiffening, the soft elastomer is able to avert *EMI*, resulting in gains of an order of magnitude. The theoretical maximum is now increased to 1.0 J/g .

What happens if ϵE_{EB}^2 is further increased? Using the reference materials of natural rubber with a constant $E_{EB} = 30.0 \text{ MV/m}$, and VHB elastomer with stretch-dependent E_{EB} , we explore the effect of varying ϵE_{EB}^2 over four orders of magnitude, for four different stiffnesses as shown in Fig. 8. As a reference, VHB has $\epsilon E_{EB}^2 = 0.037 \text{ MPa}$ at low stretch, and $\epsilon E_{EB}^2 = 2.12 \text{ MPa}$ at high stretch. It could be observed that, when the elastomer is not sufficiently stiff to avert *EMI*, increasing ϵE_{EB}^2 does nothing to improve Y_{\max} at small to moderate strains of operation. In all cases, strain-stiffening at high strains of operation improves Y_{\max} . We may summarize the roles of small strain shear stiffness μ , and the Maxwell stress at electrical breakdown ϵE_{EB}^2 as follows: At small strains of operation, $\epsilon E_{EB}^2 > \mu \epsilon_{\max}$ is

preferred, and Y_{\max} increases linearly with μ . At high strains of operation, a sufficiently stiff elastomer such that EMI is averted at all strains of operation is preferred, and Y_{\max} increases linearly with ϵE_{EB}^2 . From Fig. 8c, for a moderately stiff polymer ($\mu = 5.0 \text{ MPa}$), with $\epsilon E_{EB}^2 = 1.0 \text{ MPa}$, it is possible to convert 1.0 J/g of energy at a strain of operation of 100%. This could be realizable in the near future.

6. Conclusion

Limit state analysis is used to determine the theoretical maximum energy of conversion for a dielectric elastomer generator. Our model enables realistic operation maps to be generated for a given dielectric elastomer. The limits of operation and maximum energy of conversion can be determined from the operation map. Operation maps for existing elastomers can also be created to aid in material selection. They can be varied depending on the operating level of stretch, and practical cycles can be designed within the allowable states. Equations were established to estimate the maximum energy of conversion for a given material, with a pre-determined strain of operation. These equations enable engineers and material scientists to select and design suitable materials as dielectric elastomer generators. To ensure excellent performance in terms of energy conversion a stiff elastomer with high Maxwell stress at electrical breakdown is desired. This framework of understanding will serve as a valuable tool for material scientists and engineers to select and design the best elastomer-type materials for energy generation.

Using a similar framework, limit state analysis can also be performed for viscoelastic dielectric elastomers. This will enable the efficiency of conversion to be known at various speeds of operation. As most actuator and generator operation follows a periodic pattern, and it is generally desirable to operate at a relatively high speed to maximize power, dynamic effects must be considered in future works. Optimal operation speeds can therefore be determined that maximizes power. Operation maps for actual geometries in both actuation (diamond actuators, minimum energy configurations etc.) and energy generation (inflated membrane, rolled layers of DE, balloons etc.) can also be studied. For experimentalists, this work has provided a strong

motivation to characterize the electrical breakdown properties of various polymers (in particular, natural rubber), especially at high levels of stretch. The fatigue threshold limit for various elastomers can also be investigated, so that maximal energy of conversion can be determined for long-term, reliable operation. The range of operation in terms of maximum material deformation can also be studied using dynamic analysis, and impedance matching with external excitations and different circuit configurations. Finally, using the theoretical framework proposed in this paper, experimentalists and material scientists can work in-tandem to create new materials which are stiffer, with improved dielectric constants and dielectric strengths. A final culmination of all theoretical framework developed will greatly improve the design and operation of existing dielectric elastomer generators as energy harvesters.

Acknowledgement

This work was partially funded by the Agency for Science, Technology and Research (A*STAR), Singapore, through the sponsoring of a two-year postdoctoral visit of SJA Koh to Harvard University, and by the National Science Foundation through a grant on Soft Active Materials. Additionally the work was supported by the Austrian Science Fund and by the Austrian Marshall Plan Foundation, through the sponsoring of a half-year visit of C Keplinger to Harvard University. The work was also supported by the China Scholarship Council Foundation through the sponsoring of a one-year visit of Tiefeng Li to Harvard University.

References

1. R. A. Anderson, *Phys. Rev. B* **33**, 1302 (1986).
2. R. Pelrine, R. Kornbluh, Q. Pei, and J. Joseph, *Science* **287**, 836 (2000).
3. G. Kofod, M. Paajanen, and S. Bauer, *Appl. Phys. A* **85**, 141 (2006).
4. N. Galler, H. Ditzbacher, B. Steinberger, A. Hohenau, M. Dansachmuller, F. Camacho-Gonzales, S. Bauer, J. R. Krenn, A. Leitner, and F. R. Aussenegg, *Appl. Phys. B* **85**, 7 (2006).
5. G. Kovacs, L. During, S. Michel, and G. Terrasi, *Sens. Actuators A* **155**, 299 (2009).
6. X. Zhao, and Z. Suo, *Appl. Phys. Lett.* **93**, 251902 (2008).

7. C. Keplinger, M. Kaltenbrunner, N. Arnold, and S. Bauer, *Appl. Phys. Lett.* **92**, 192903 (2008).
8. C. Keplinger, M. Kaltenbrunner, N. Arnold, and S. Bauer, *Proc. Nat. Acad. Sci.* **107**, 4505 (2010).
9. R. Pelrine, R. Kornbluh, J. Eckerle, P. Jeuck, S. Oh, Q. Pei, and S. Stanford, *Proceedings of SPIE Electroactive Polymer Actuators and Devices*, Newport, CA, March 2001, Vol. 4329, p. 148.
10. S. J. A. Koh, X. Zhao, and Z. Suo, *Appl. Phys. Lett.* **94**, 262902 (2009).
11. S. Chiba, M. Waki, R. Kornbluh, and R. Pelrine, *Proceedings of SPIE Electroactive Polymer Actuators and Devices*, San Diego, CA, March 2008, Vol. 6927, p. 692715.
12. C. Jean-Mistral, S. Basrour, and J. J. Chaillout, *Proceedings of SPIE Electroactive Polymer Actuators and Devices*, San Diego, CA, March 2008, Vol. 6927, p. 692716.
13. Y. H. Iskandarani, R. W. Jones, and E. Villumsen, *Proceedings of SPIE Electroactive Polymer Actuators and Devices*, San Diego, CA, March 2009, Vol. 7287, p. 72871Y.
14. P. Lochmatter, G. Kovacs, and M. Wissler, *Smart Mater. Struct.* **16**, 477 (2007).
15. L. R. G. Treloar, *The Physics of Rubber Elasticity*, p. 101 (Clarendon Press, Oxford, 1975).
16. E. M. Arruda, and M. Boyce, *J. Mech. Phys. Solids* **41**, 389 (1993).
17. G. Kofod, *Dielectric Elastomer Actuators*, Ph.D. Thesis, The Technical University of Denmark, Sept. 2001, p. 72.
18. J. S. Plante and S. Dubowsky, *Int. Solid Struct.* **43**, 7727 (2006)
19. R. M. Wissler and E. Mazza, *Sens. Actuators A* **138**, 384 (2007).
20. J. Kymissis, C. Kendall, J. Paradiso, and N. Gershenfield, *Digest of the Second IEEE International Conference on Wearable Computing*, August 2002, pp. 132.
21. H. Sodano, D. Inman, and G. Park, *J. Intell. Mater. Syst. Struct.* **16**, 799 (2005).
22. K. Ren, Y. Liu, H. Hofmann, and Q. M. Zhang, *Appl. Phys. Lett.* **91**, 132910 (2007).
23. K. H. Stark, and C. G. Garton, *Nature* **176**, 1225 (1955).
24. M. Moscardo, X. Zhao, Z. Suo, and Y. Lapusta, *J. Appl. Phys.* **104**, 093503 (2008).
25. X. Zhao and Z. Suo, *Appl. Phys. Lett.* **91**, 061921 (2007).

26. S. J. A. Koh, Proceedings of MRS Symposium Z, Boston, MA, 30 Nov. – 4 Dec. 2009, Vol. 1218E.
27. R. E. Pelrine, R. D. Kornbluh, and J. P. Joseph, *Sens. Actuators A* **64**, 77 (1998).
28. J. D. Vogan, *Development of Dielectric Elastomer Actuators for MRI Devices*, Masters Thesis, Massachusetts Institute of Technology, June 2004, p. 15.
29. J. J. O'Dwyer, *The Theory of Dielectric Breakdown of Solids*, p. 123 (Clarendon Press, Oxford, 1964).
30. M. Kolloosche, M. Melzer, A. Becker, H. Stoyanov, D. N. McCarthy, H. Ragusch, and G. Kofod, Proceedings of SPIE Electroactive Polymer Actuators and Devices, San Diego, CA, April 2009, Vol. 7287, p. 728729.
31. A. N. Norris, *Appl. Phys. Lett.* **92**, 026101 (2008).
32. X. Zhao, W. Hong and Z. Suo, *Phys. Rev. B* **76**, 134113 (2007).
33. W. Kuhn, and F. Grün, *Kolloidzschr* **101**, 248 (1942).
34. S. M. Ha, W. Yuan, Q. Pei, R. Pelrine, and S. Stanford, *Adv. Mater.* **18**, 887 (2006).
35. S. M. Ha, W. Yuan, Q. Pei, R. Pelrine, and S. Stanford, *Smart Mater. Struct.* **16**, S280 (2007).
36. K. Jung, J. Lee, M. Cho, J. C. Koo, J. Nam, Y. Lee, and H. R. Choi, *Smart Mater. Struct.* **16**, S288 (2007).
37. Z. Suo, and J. Zhu, *Appl. Phys. Lett.* **95**, 232909 (2009).
38. P. Brochu, and Q. Pei, *Macromol. Rapid Commun.* **31**, 10 (2010).
39. G. Kofod, P. Sommer-Larsen, R. Kornbluh, and R. Pelrine, *J. Int. Mater. Sys. Struct.* **14**, 787 (2003).
40. D. R. Lide, *CRC Handbook of Chemistry & Physics 79th Ed.*, p. 15 (CRC Press, Boca Raton, 1998).
41. T. He, X. Zhao, and Z. Suo, *J. Appl. Phys.* **106**, 083522 (2009).
42. G. Kofod, W. Wirges, M. Paaanen, and S. Bauer, *Appl. Phys. Lett.* **90**, 081916 (2007).

Figures

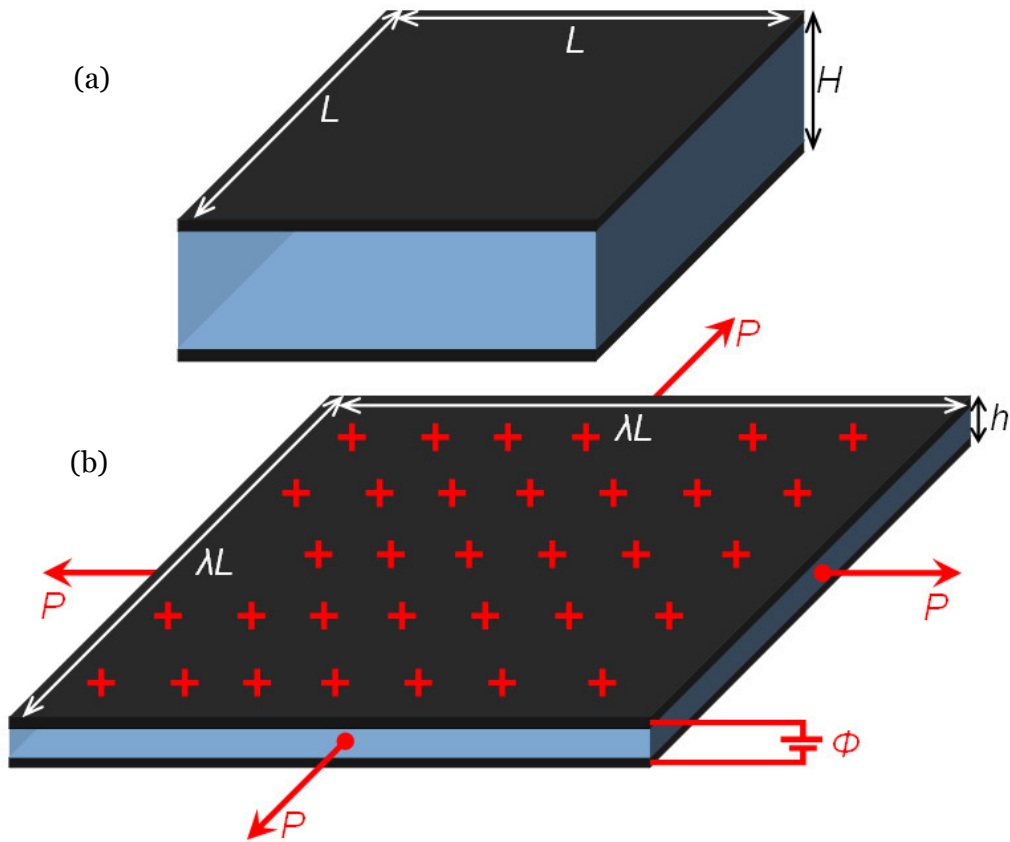


Figure 1. Operation of a dielectric elastomer transducer. A membrane of a dielectric elastomer is sandwiched between compliant electrodes. (a) In the reference state, the membrane is subject to neither force nor voltage, and is undeformed. (b) In the activated state, the membrane is subject to equal-biaxial force P in its plane and voltage Φ through its thickness. The membrane expands the area by a factor of λ^2 , and reduces the thickness to $h = H\lambda^{-2}$. Electrons flow through the external circuit, resulting in positive and negative electric charges, $\pm Q$, on the two electrodes.

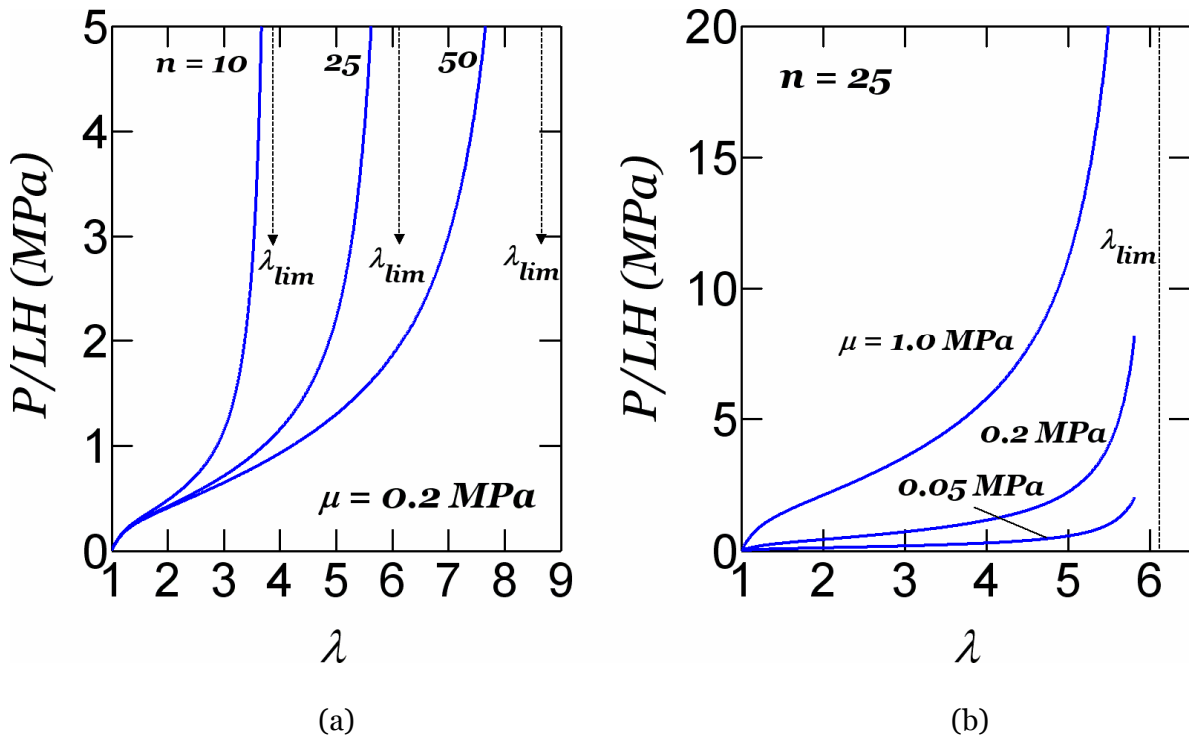


Figure 2. The relation between the stretch λ and the equal-biaxial nominal stress P/LH . (a) The number of links in each polymer chain, n , sets the limit stretch λ_{lim} . (b) The small-strain modulus μ sets the amplitude of the nominal stress.

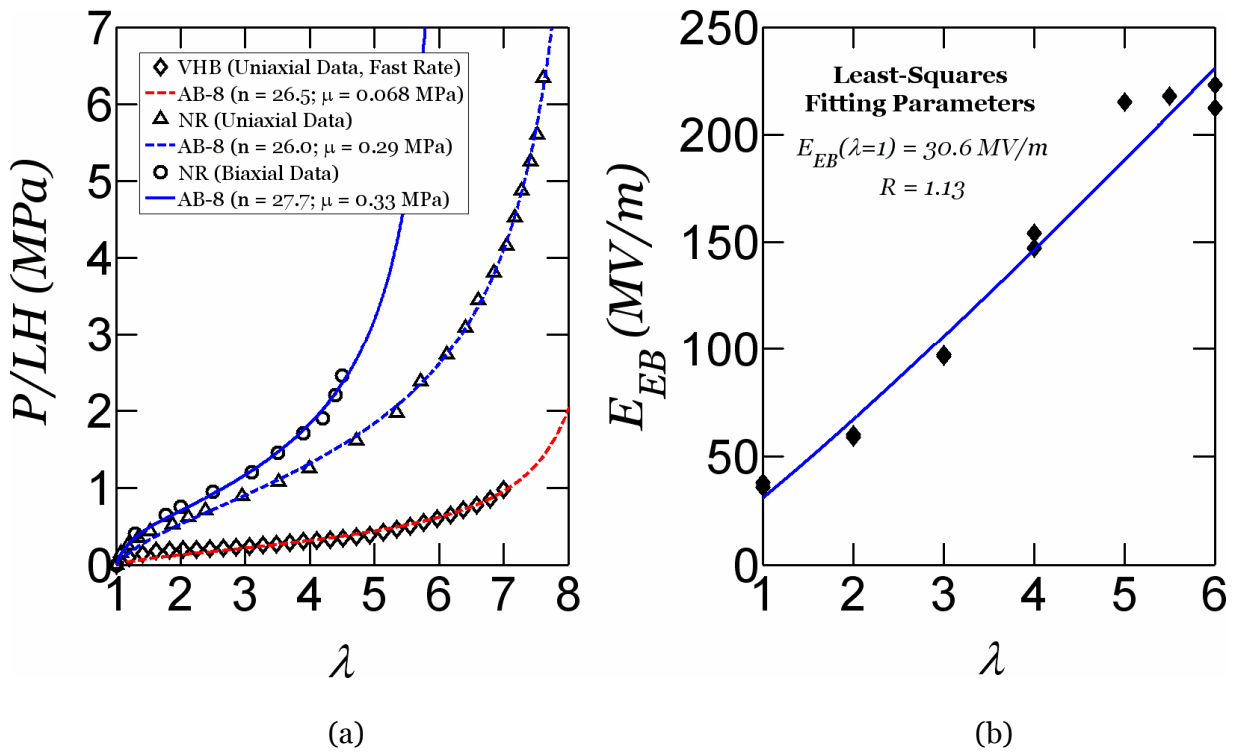


Figure 3. Experimental data fit of (a) force-displacement curves for natural rubber (NR, Treloar, 1944) and VHB acrylic elastomer under fast uniaxial loading (VHB, Planté & Dubowsky, 2006), using the Arruda-Boyce 8-chain model (AB-8) and (b) stretch-dependent electrical breakdown field for VHB (Kofod et. al., 2003; Planté & Dubowsky, 2006).

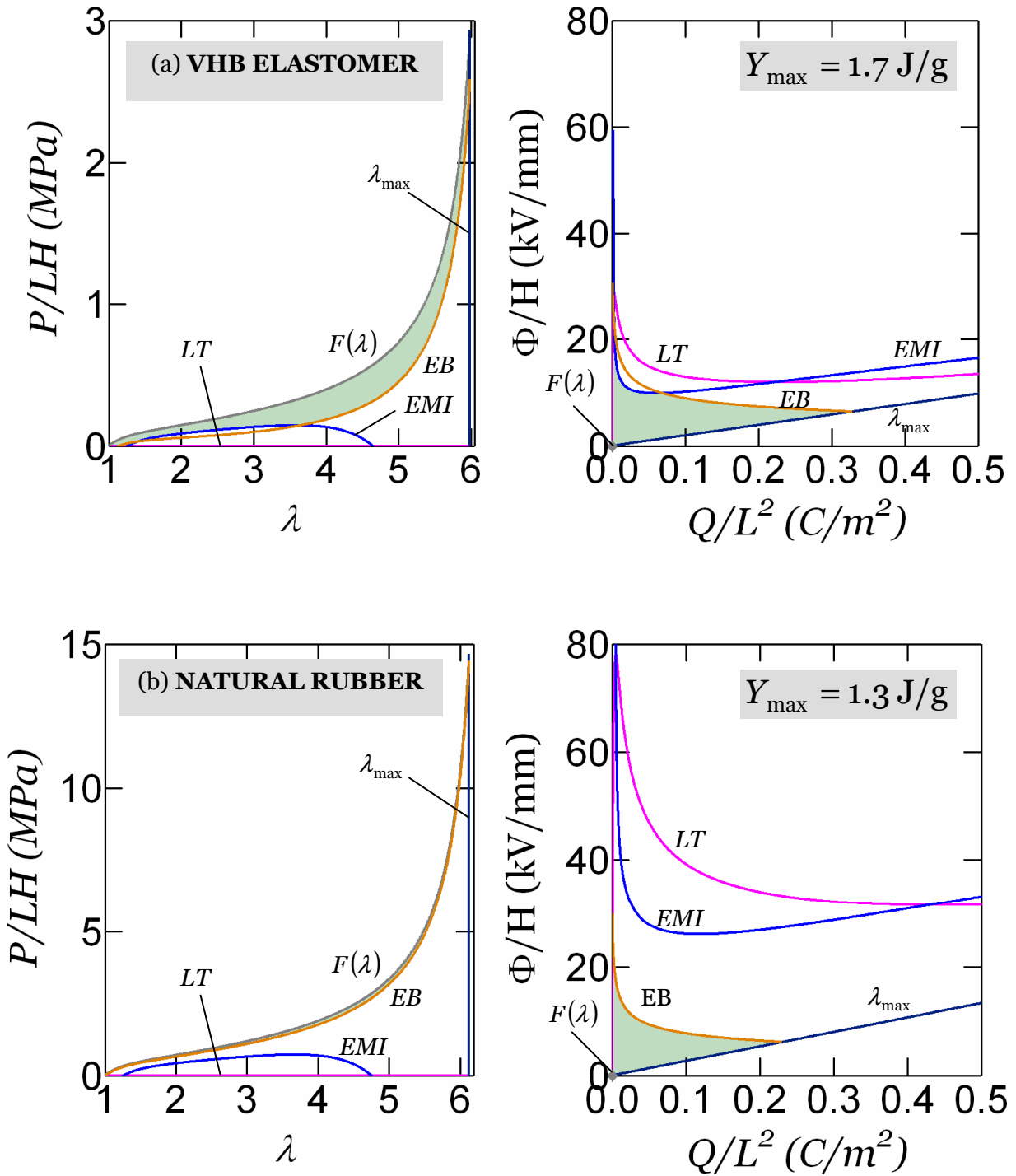
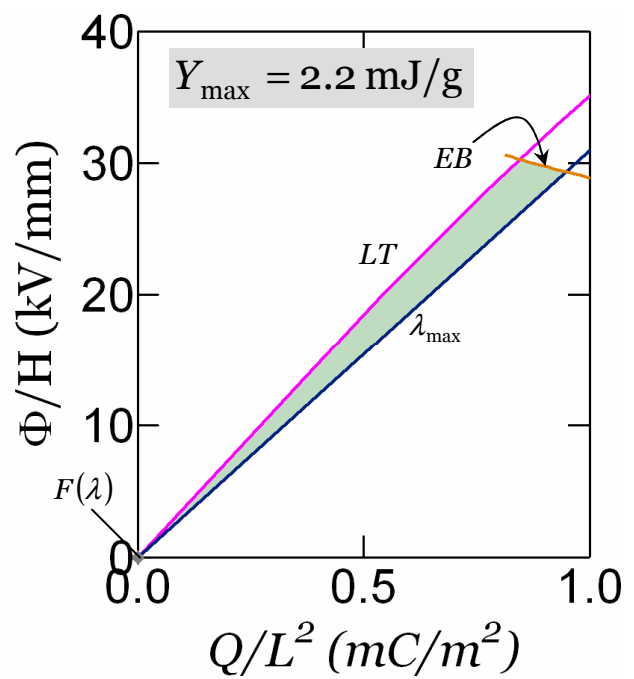
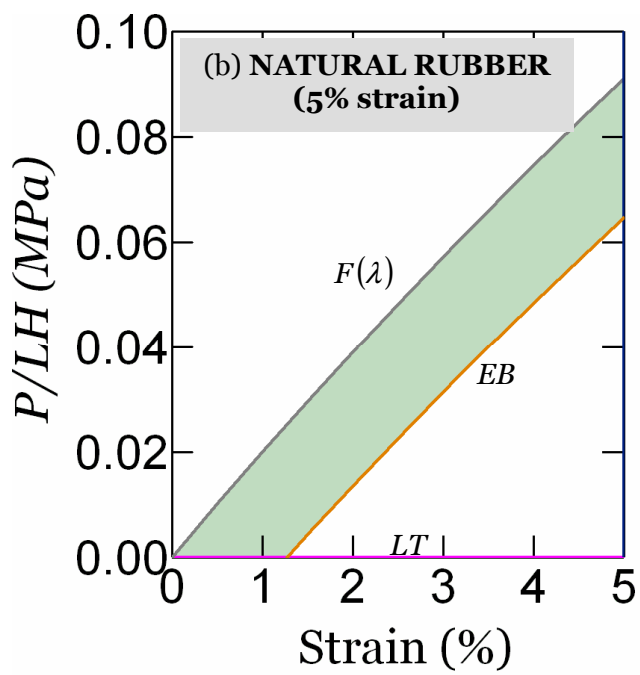
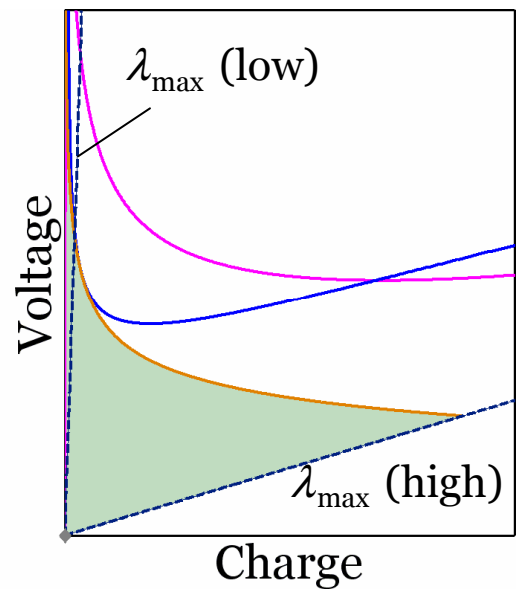
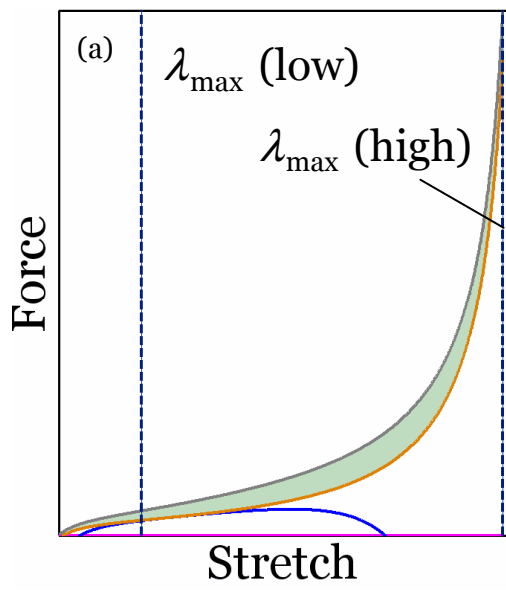


Figure 4. Limit states define a shaded region of allowable states on the force-displacement plane, and the voltage-charge plane for (a) VHB elastomer and (b) natural rubber, under equal-biaxial loading. The abbreviations on the plot refer to the following limit states: λ_{max} is maximum stretch, EB is electrical breakdown, EMI is electromechanical instability, LT is loss of tension, and $F(\lambda)$ is the nominal stress-strain curve, which defines the thermodynamic stability limit. In these plots, it was assumed that the elastomer is stretched up to near its limit stretch

during operation. The area of the shaded region gives the theoretical maximum energy of conversion for the elastomer. These plots are termed *operation maps*.



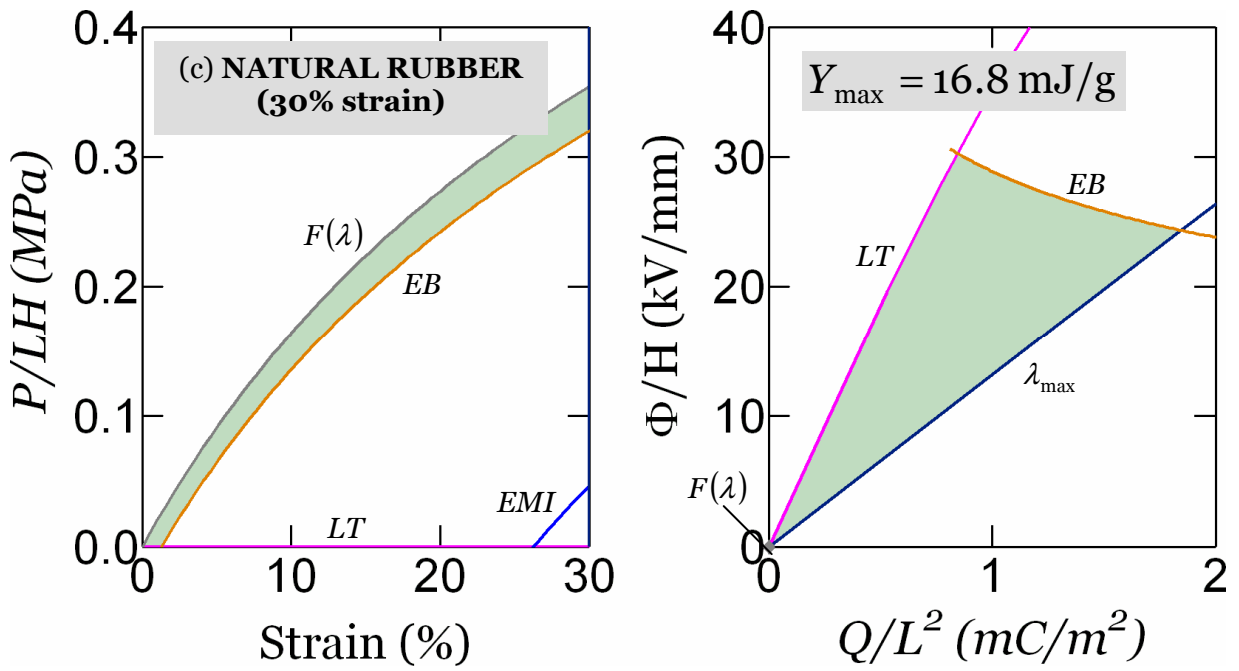


Figure 5. Operation maps for dielectric elastomer when the maximum stretch (λ_{max}) is varied (a) The shaded area is reduced due to the leftward translation of the λ_{max} line on the P - λ plane, and anti-clockwise rotation of the same line, about the origin on the Φ - Q plane; (b) Operation map for natural rubber (Fig. 4b) when the maximum stretch is limited to $\lambda_{max} = 1.05$ (5% strain) and (c) Operation map for natural rubber when the maximum stretch is limited to $\lambda_{max} = 1.3$ (30% strain).

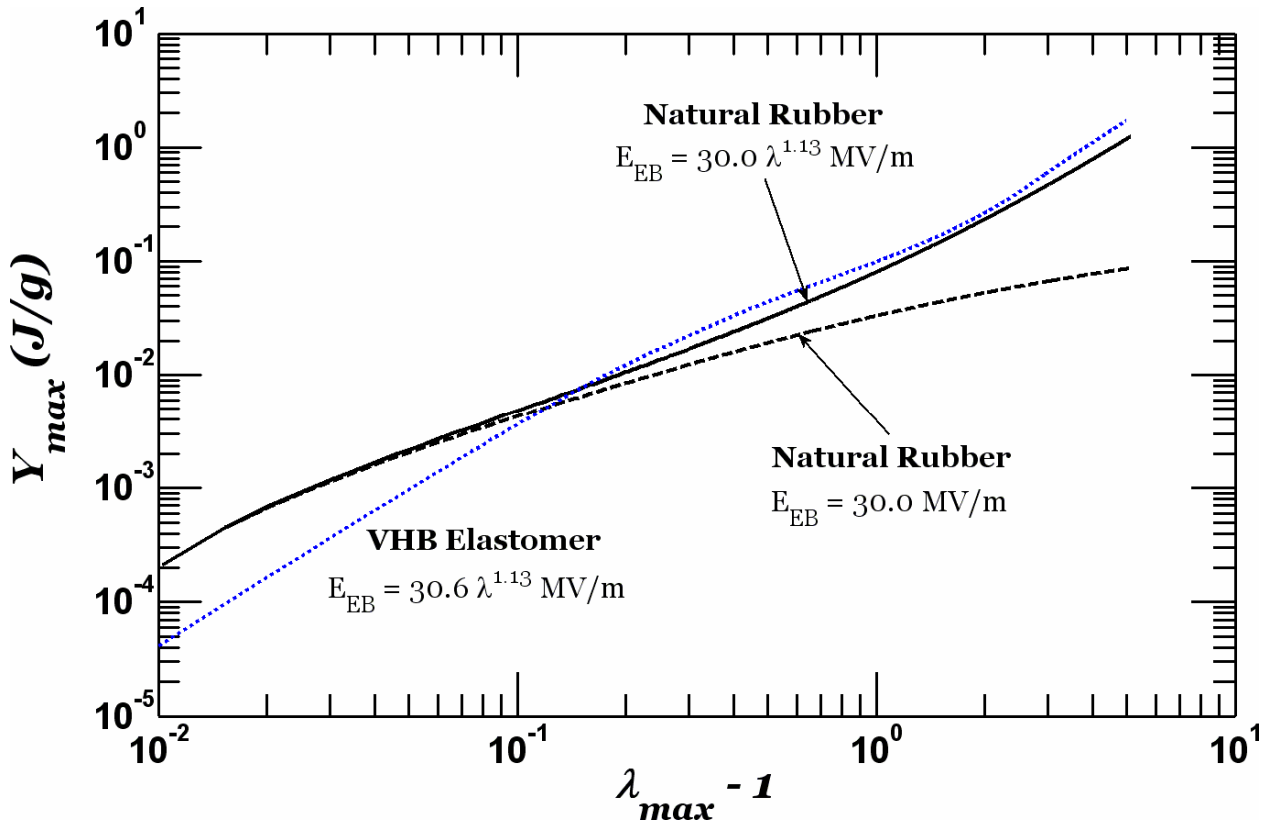


Figure 6. Maximum energy of conversion over the entire spectrum of operating strains for VHB elastomer, NR with stretch-dependent dielectric strength, and NR with stretch-independent dielectric strength. The maximum energy of conversion (Y_{max}) spans at least two orders of magnitude over the entire spectrum of operating strains.

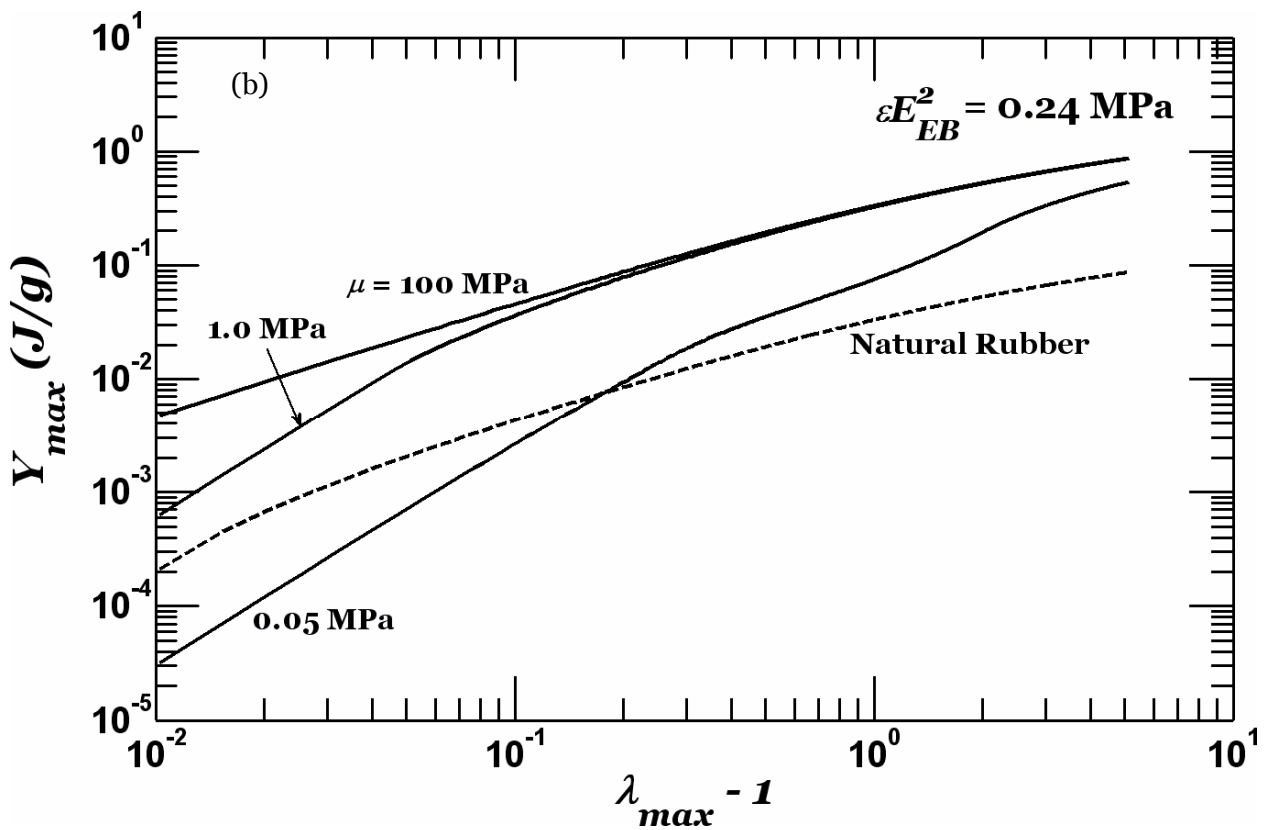
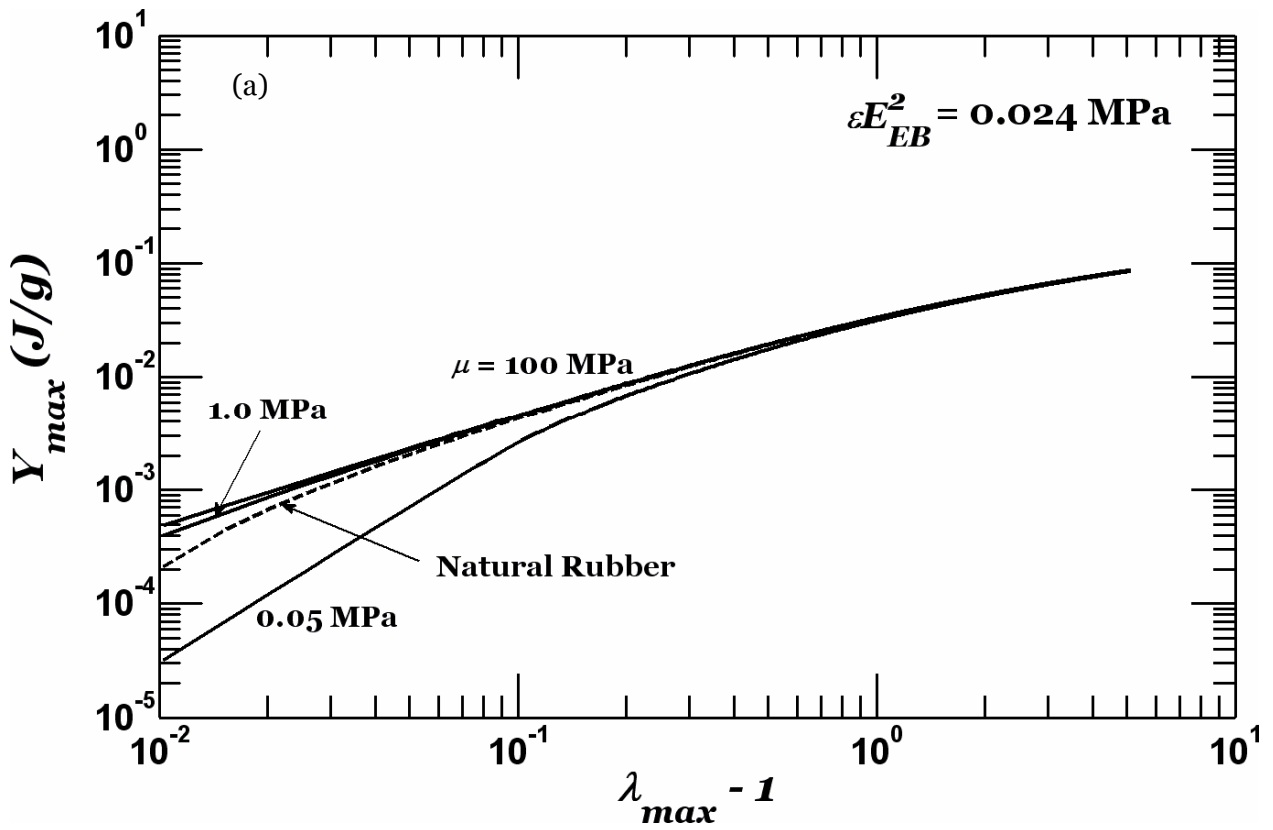
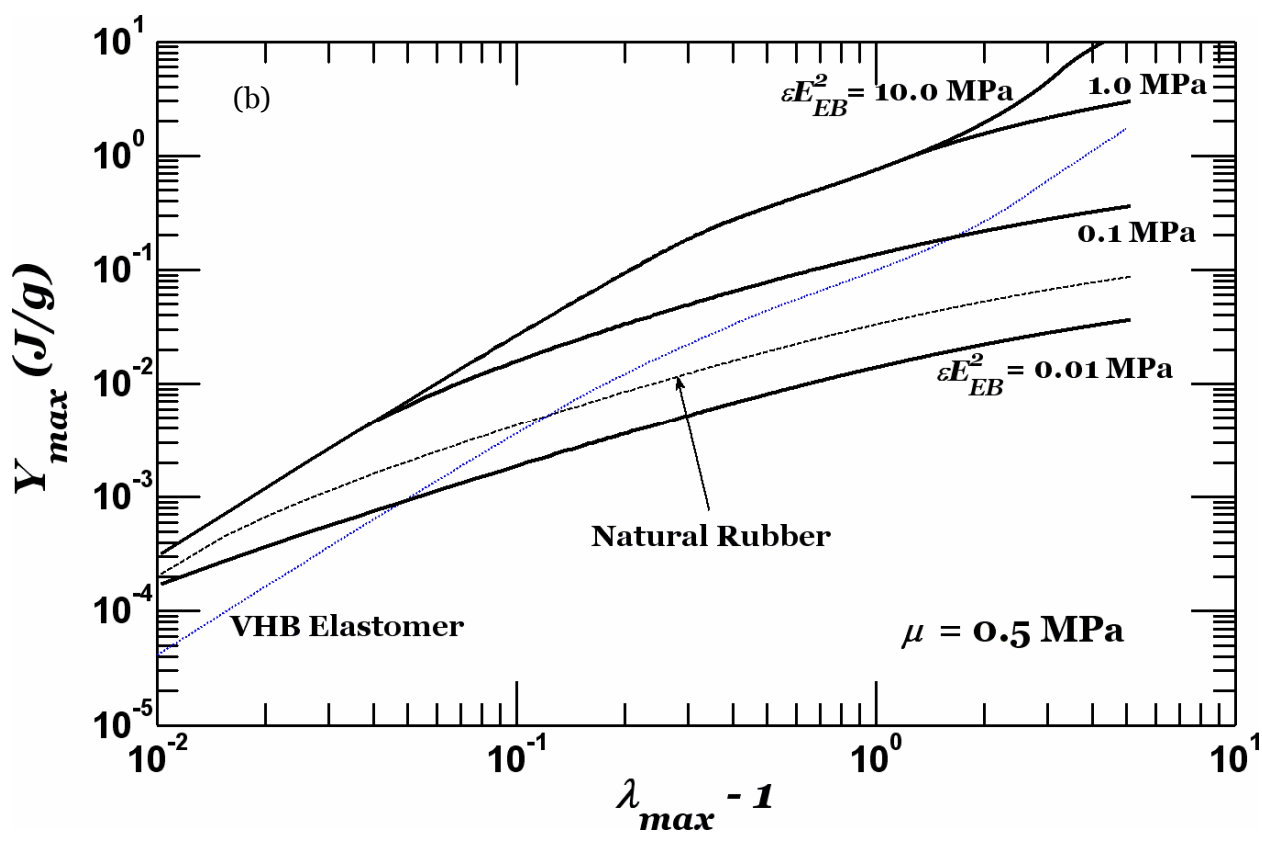
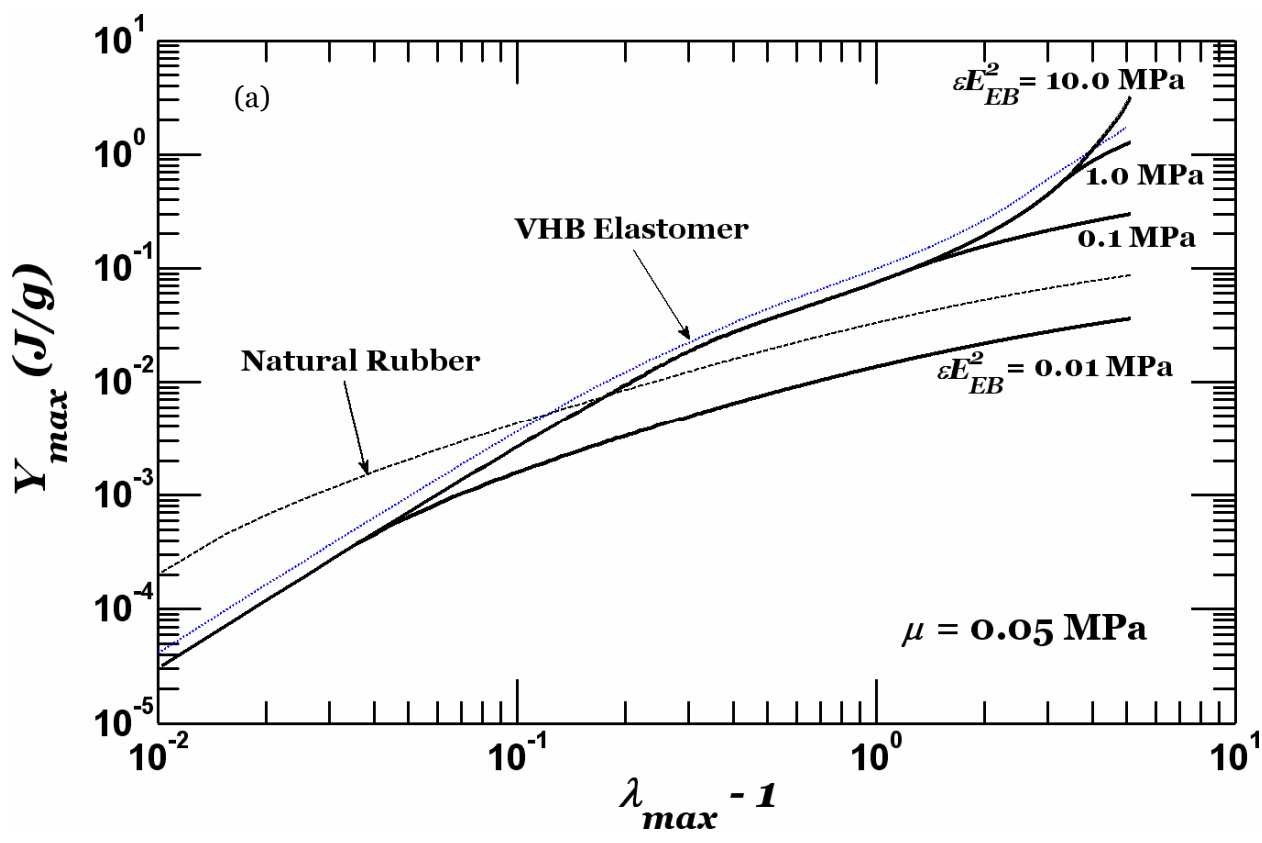


Figure 7. Exploring effect of material parameters μ and ϵE_{EB}^2 on the maximum energy of conversion Y_{max} . The material parameters for natural rubber with $E_{EB} = 30.0 \text{ MV/m}$ is taken

as reference. For a fixed εE_{EB}^2 , μ is varied. (a) The value εE_{EB}^2 of natural rubber is used and (b) The value εE_{EB}^2 of ten times that of natural rubber is used. A one order of magnitude increase in Y_{\max} is possible due to an equivalent increase in εE_{EB}^2 . For a soft elastomer ($\mu = 0.05$ MPa), maximum energy for the higher εE_{EB}^2 is predominantly controlled by EMI .



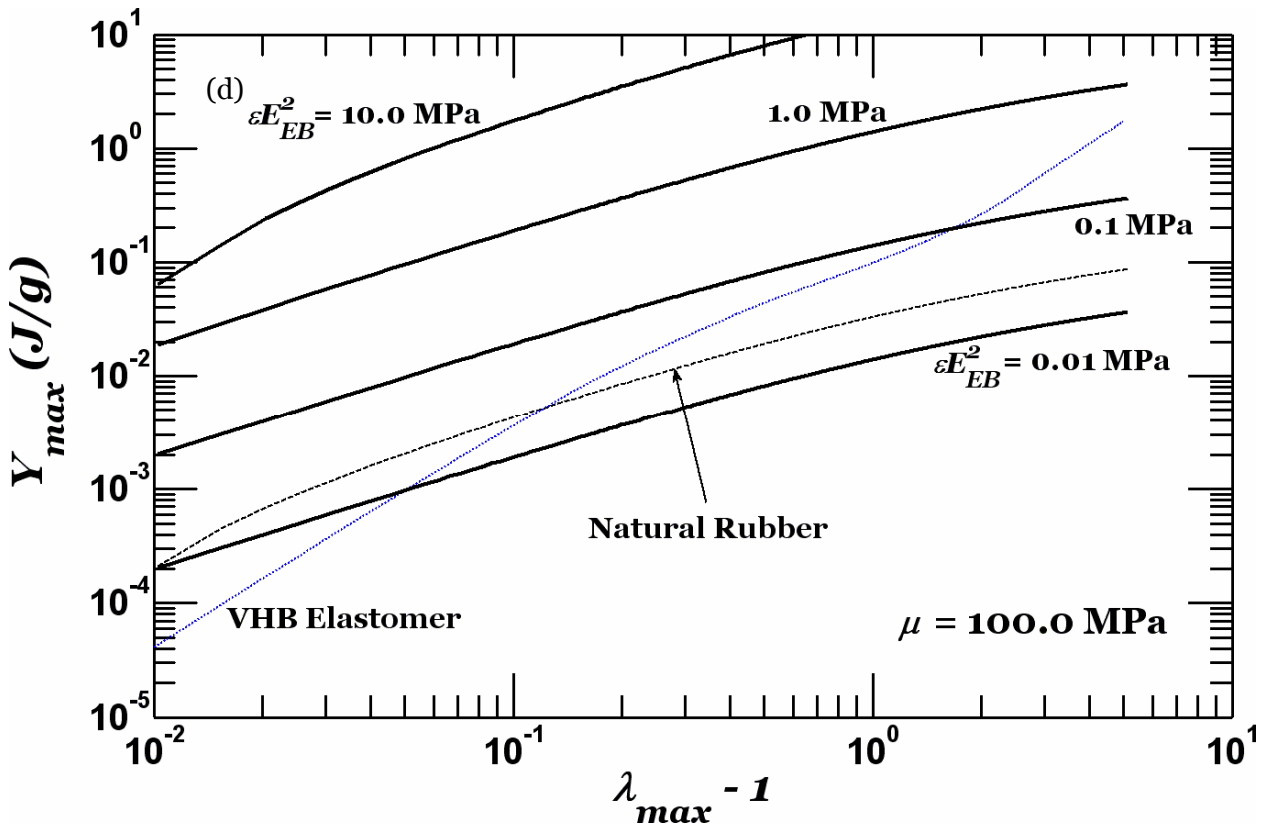
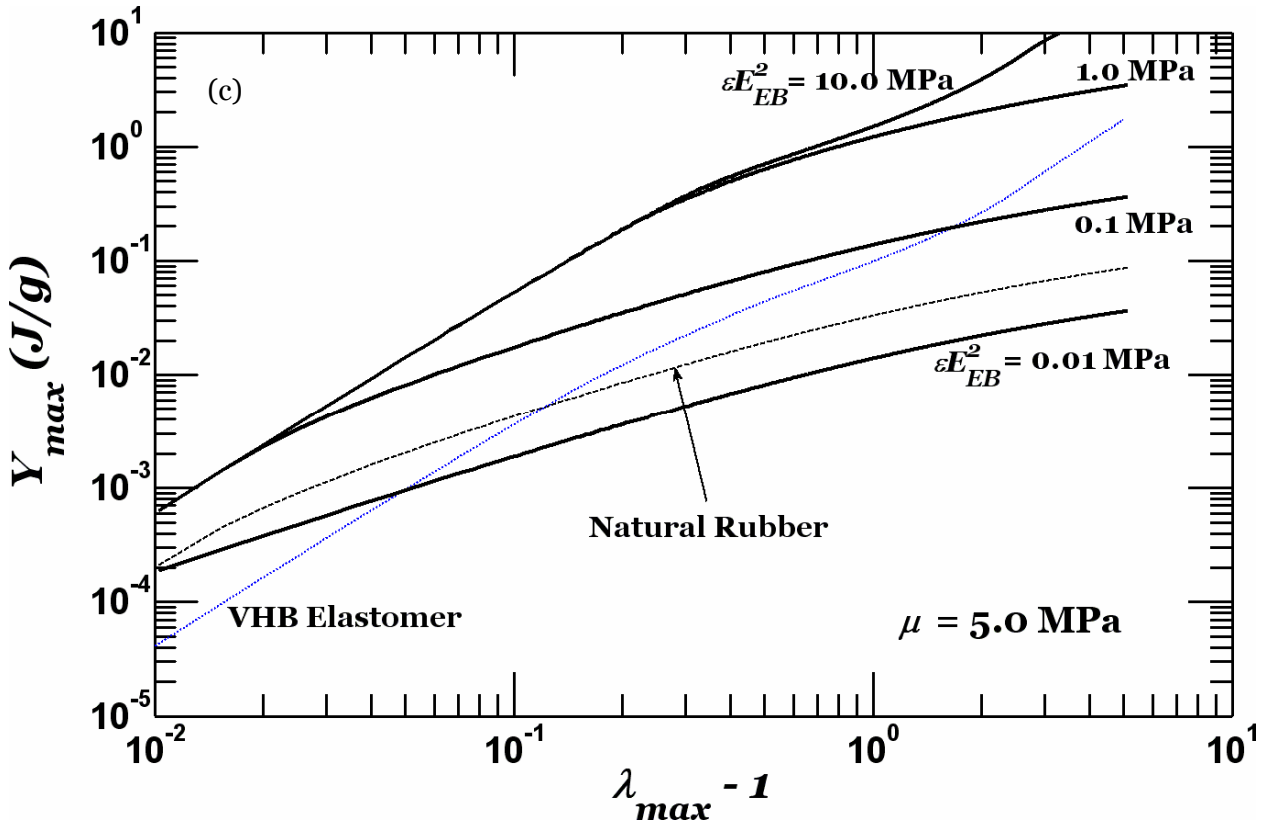


Figure 8. Exploring effect of material parameters μ and ϵE_{EB}^2 on the maximum energy of conversion Y_{max} . The material parameters for natural rubber with $E_{EB} = 30.0$ MV/m (dashed

line), and VHB elastomer (dotted line) are taken as references. For a fixed μ , εE_{EB}^2 is varied. Four stiffnesses were chosen (a) $\mu = 0.05$ MPa ; (b) $\mu = 0.5$ MPa ; (c) $\mu = 5.0$ MPa and (d) $\mu = 100$ MPa .

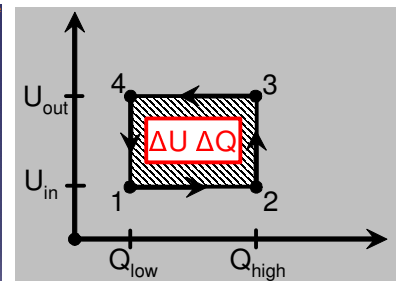
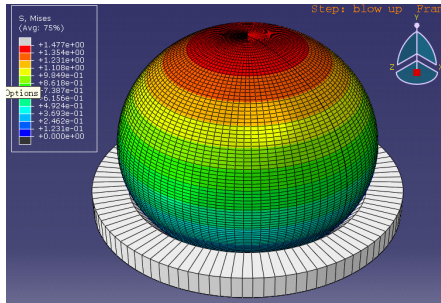
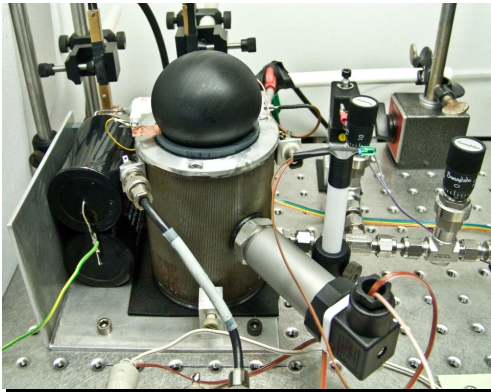
Appendix 1



HARVARD
School of Engineering
and Applied Sciences



JOHANNES KEPLER
UNIVERSITY LINZ | JKU



ENERGY HARVESTING

Aptitude of Dielectric Elastomer Transducers for Energy Harvesting Generators

Christoph Keplinger^{1,2}, Tiefeng Li², Jian Zhu² and Zhigang Suo²

Phillip Mächler¹, Martin Kaltenbrunner¹, Reinhard Schwödiauer¹, Nikita Arnold¹ and Siegfried Bauer¹

FWF

AUSTRIAN
MARSHALL PLAN FOUNDATION
VIENNA | AUSTRIA

1) Soft Matter Physics Department

Johannes Kepler University,

Linz, Austria

2) School of Engineering and Applied Sciences,

Harvard University,

Cambridge, Massachusetts, USA

Christoph Keplinger

2010 MRS Spring Meeting, San Francisco

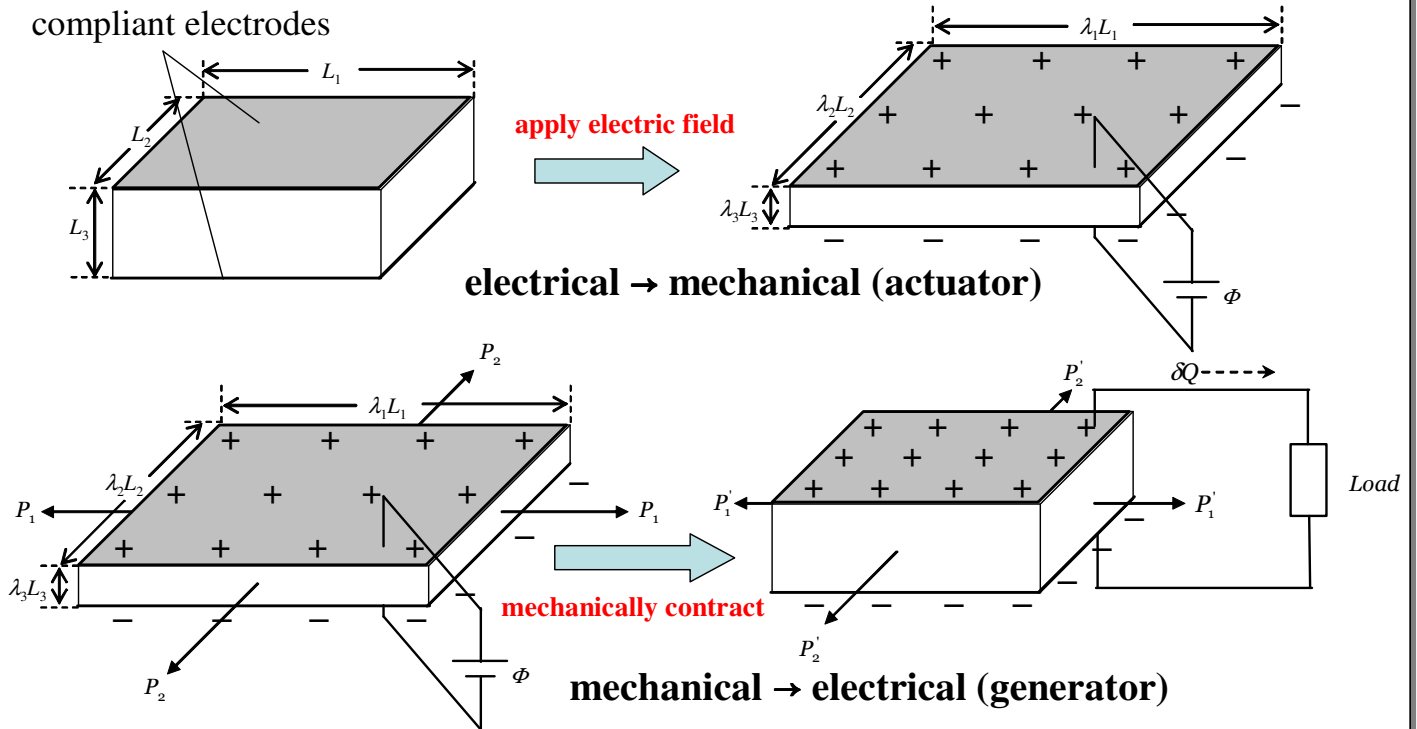
Soft Matter Physics





Dielectric Elastomer Transducers

compliant electrodes





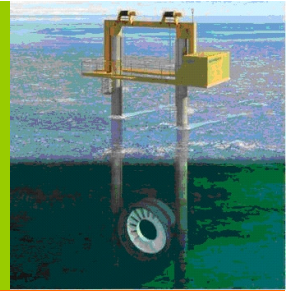
Dielectric Elastomer Generators

large-scale
(*kV-MV*
output)

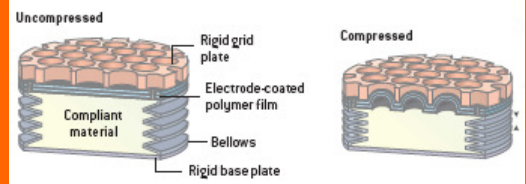
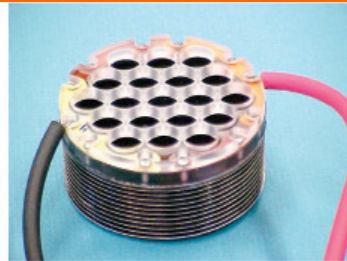


ocean wave
energy
harvesting

patents by SRI
International &
AMI

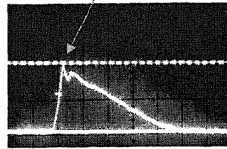
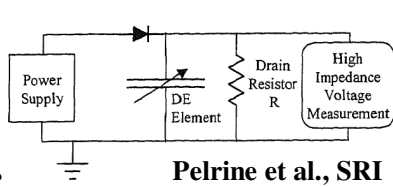


small-scale
(*mV-V*
output)



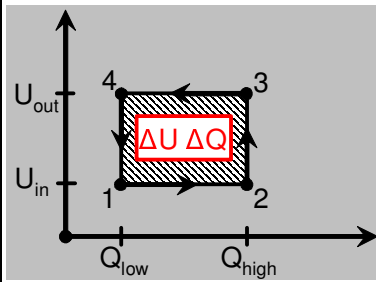
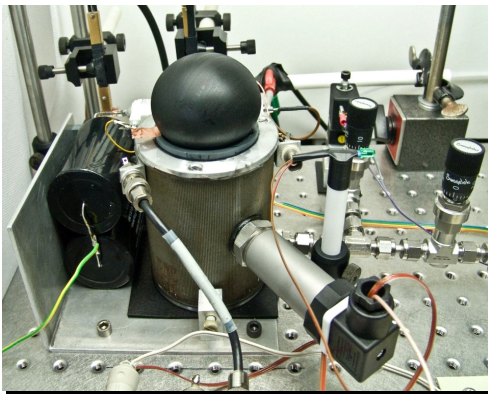
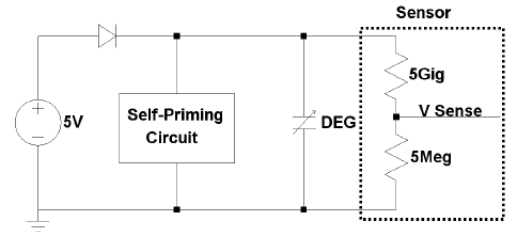


Dielectric Elastomer Generators

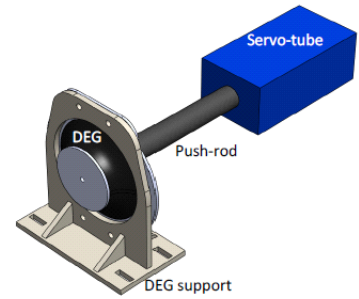


Pelrine et al., SRI

*basic
research*

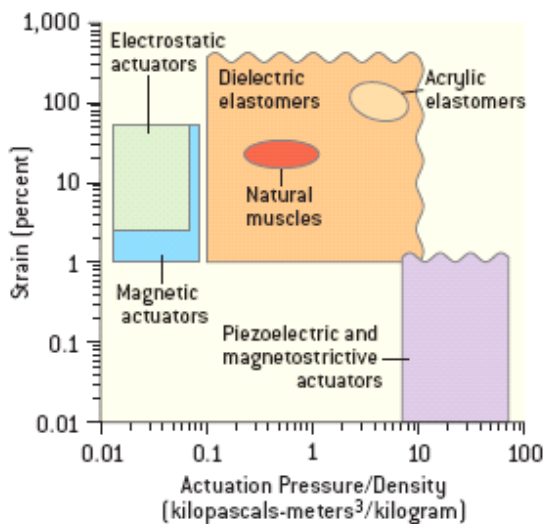


SoMaP, Linz



Anderson et al., New Zealand

Why Dielectric Elastomer Transducers?



^aR. Pelrine et. al. (2001), *Proc. SPIE* **4329**, 148

^bS. Ashley (2003), *Scientific American* **289**, 52

- high energy density
 - orders higher than parallel technologies^{a,b}
- light-weight, soft and compliant
- economically interesting
 - inexpensive materials
 - rust free → offshore, low maintenance costs
- wave energy harvesting
 - concentrated energy stored in waves
 - potential unclear
 - good impedance matching

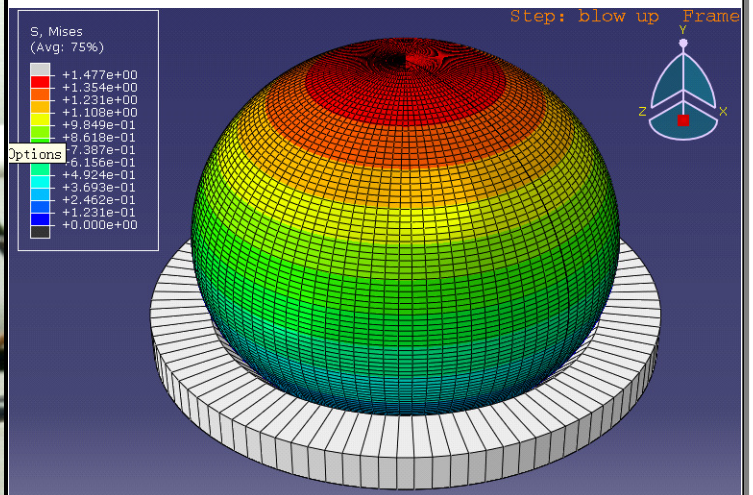


Motivation

- lack of experiments
 - to estimate full potential of the technology
 - to improve basic understanding
- well defined thermodynamic cycle
 - in work conjugate voltage charge plots
 - operate between two charge reservoirs of different electrical potential
- What is the ideal deformation mechanism?
 - theoretically, equibiaxial deformation is ideal
 - how to realize experimentally?



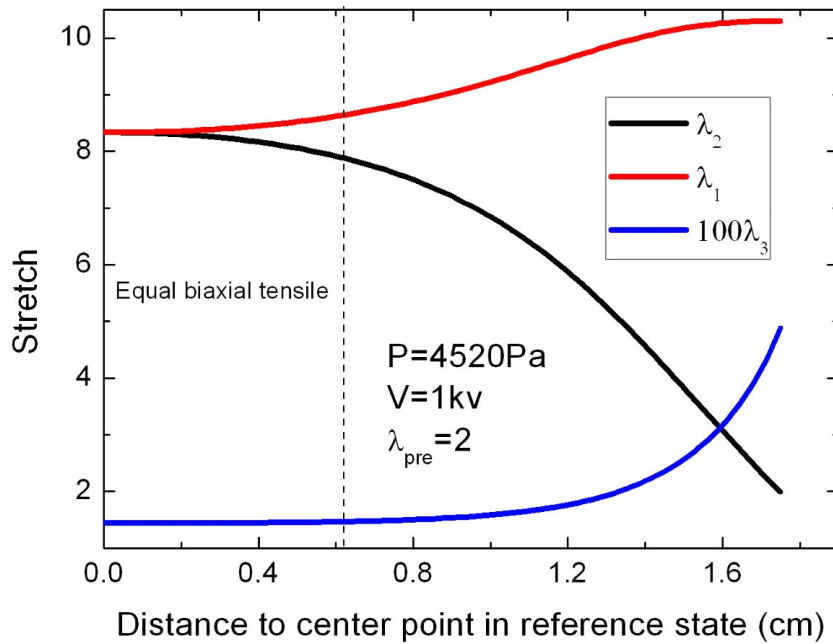
Inflation of a dielectric elastomer membrane





Inflation of a dielectric elastomer membrane

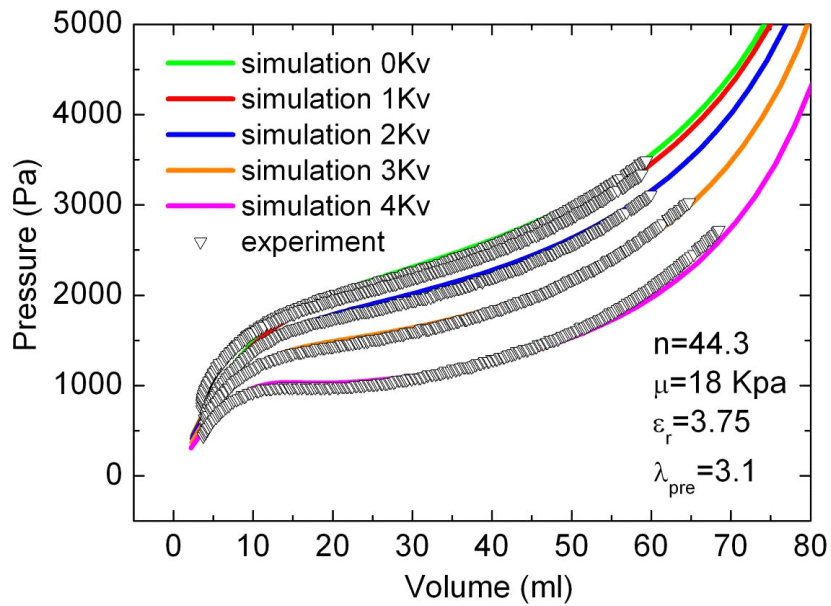
3M™VHB™4910 acrylic elastomer tape

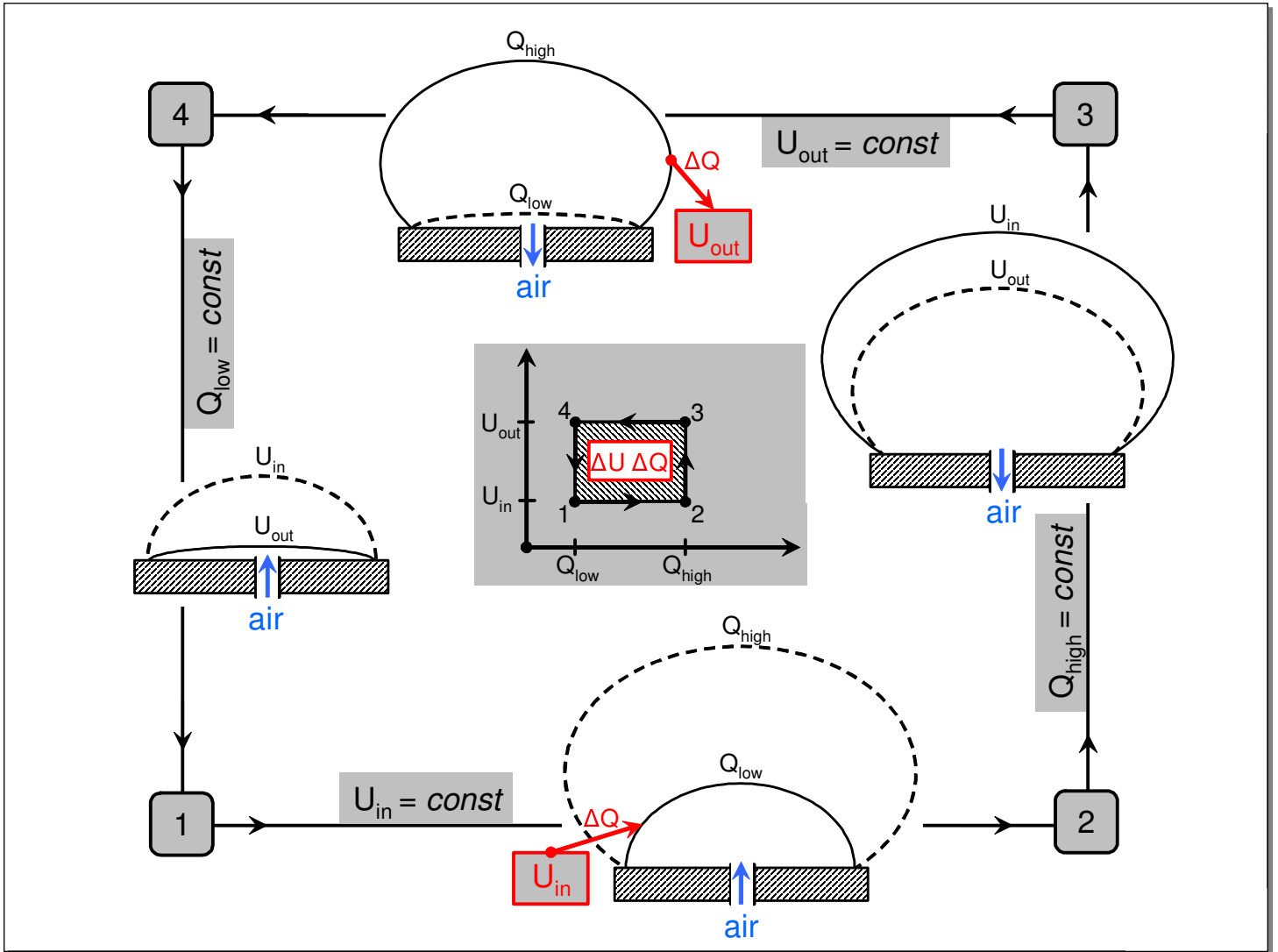




Inflation of a dielectric elastomer membrane

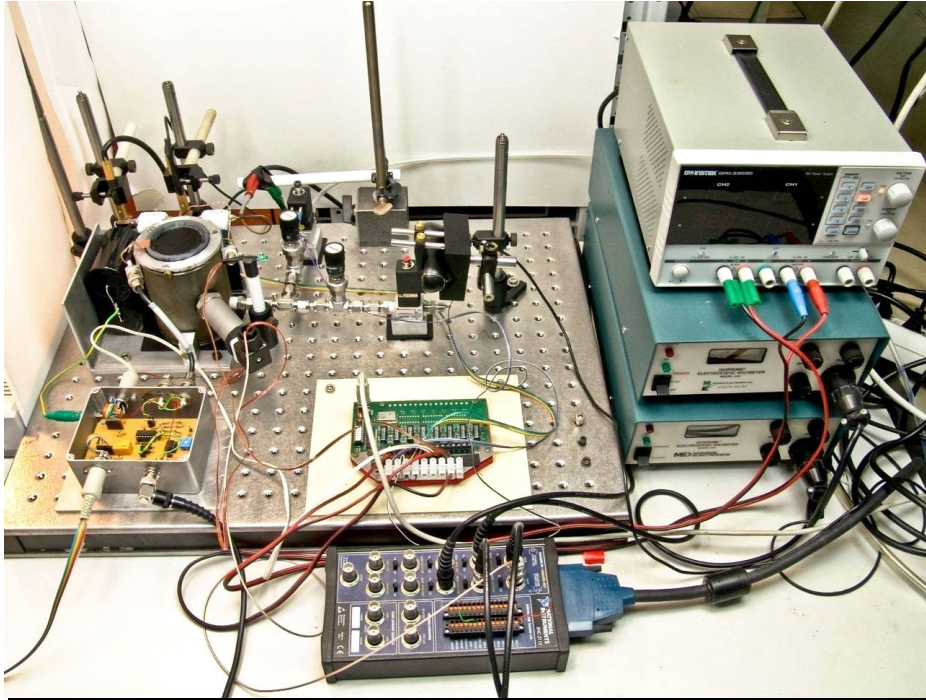
3M™VHB™4910 acrylic elastomer tape





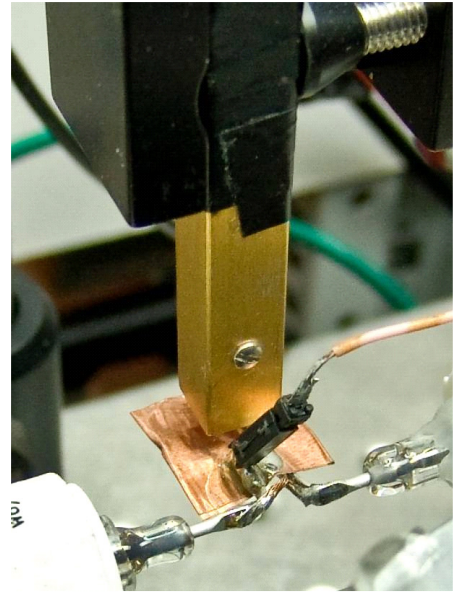
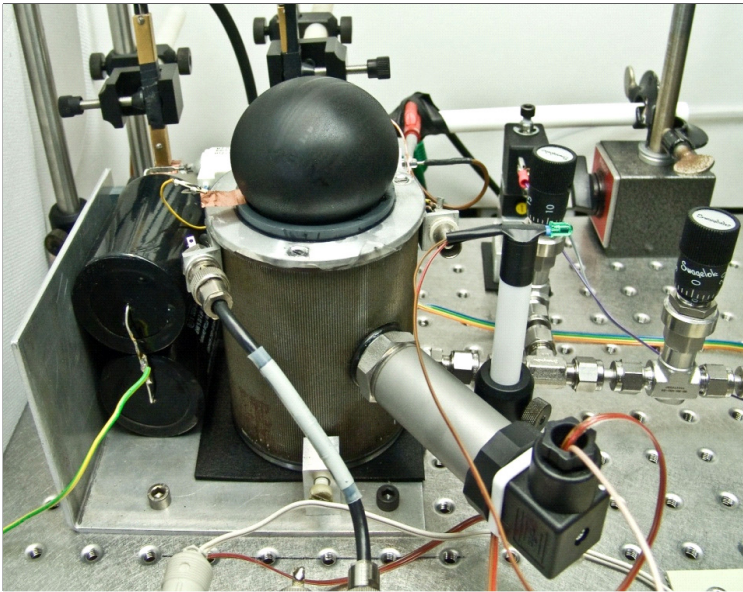


Experimental Setup



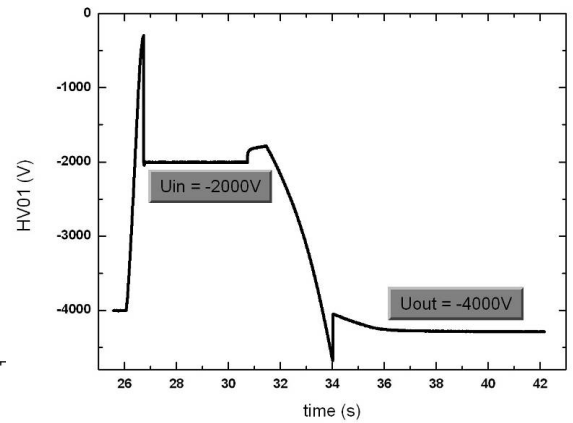
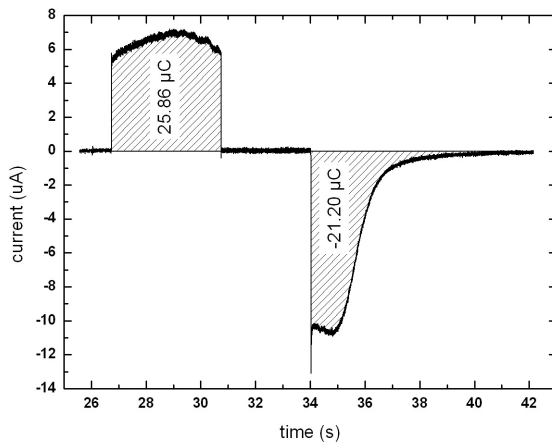


Experimental Setup

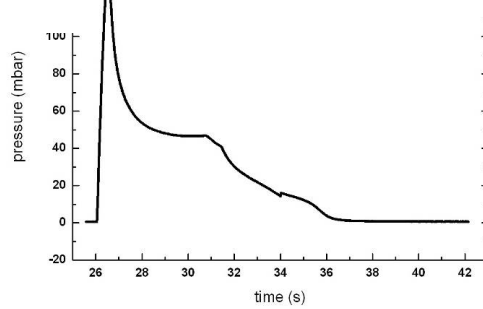




First results



3M™VHB™4910
acrylic elastomer tape

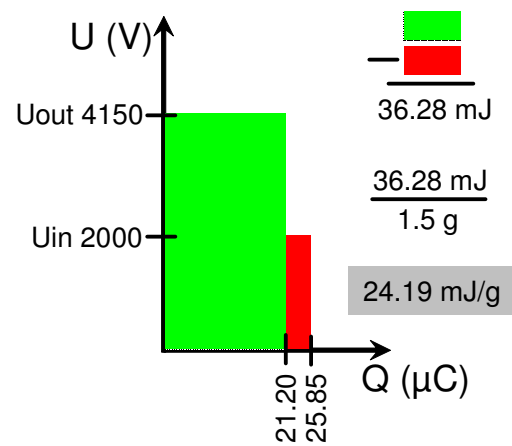
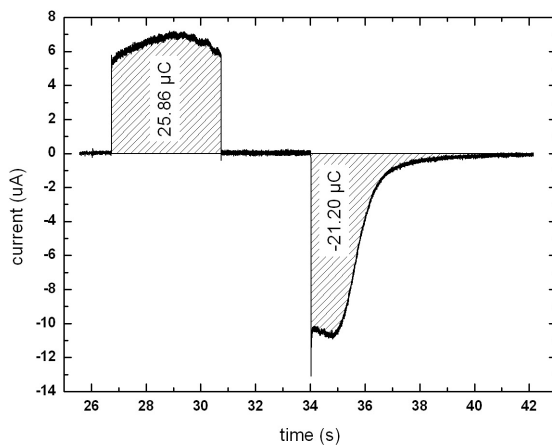


Christoph Keplinger



First results

3M™VHB™4910 acrylic elastomer tape

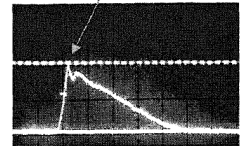
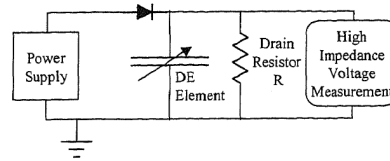


→ Energy of conversion for one cycle: 24.19 mJ/g

How does that value compare?

3M™VHB™4910 acrylic elastomer tape

- Pelrine et al.: 400mJ/g ?
 - operating conditions not specified



^aR. Pelrine et. al. (2001), *Proc. SPIE* 4329, 148

- competing technologies
 - 130mJ/g advanced single crystal ceramics^a
 - electromagnetics: peak energy density 40mJ/g ^a
- Where are the theoretical limits?

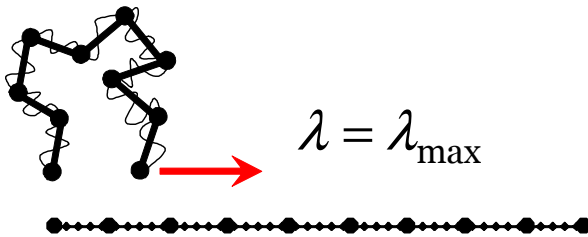


Limits of operation – failure modes

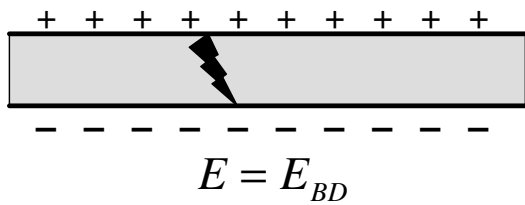
ultimate failure – destroys device

may lead to ultimate failure

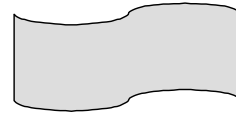
- maximal stretch, rupture



- electrical breakdown



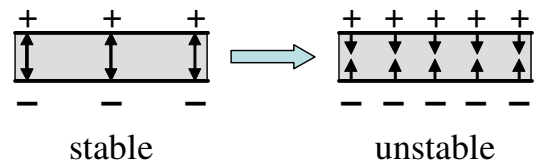
- loss of tension



or $s_1 = 0$
 $s_2 = 0$

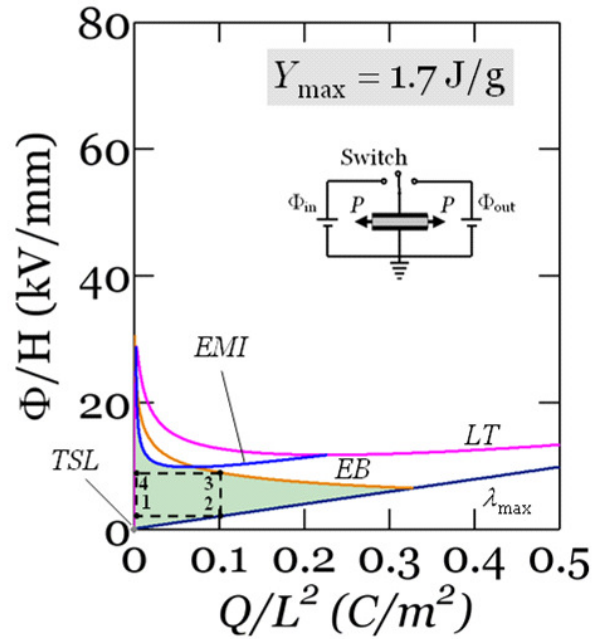
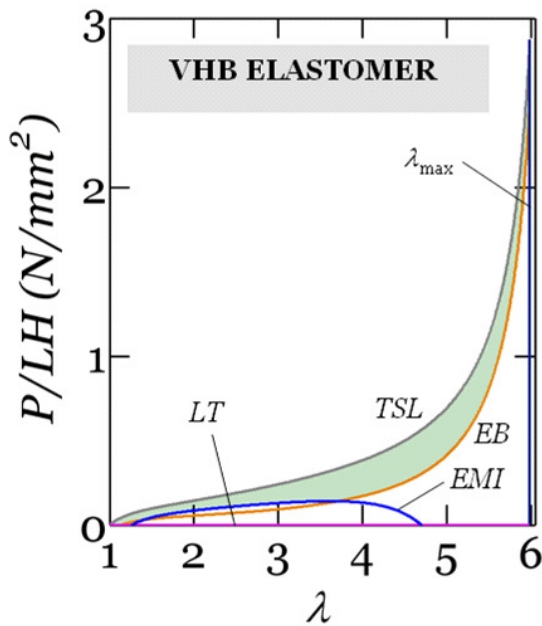


- electromechanical instability – pull-in effect





Theoretical limits for 3M™VHB™4910 (biaxial)

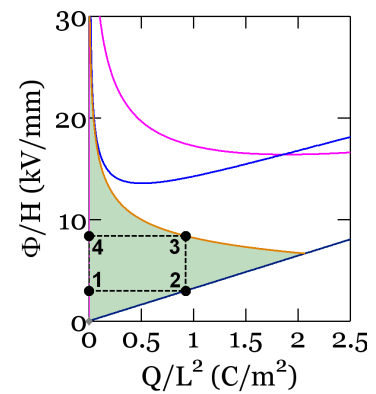
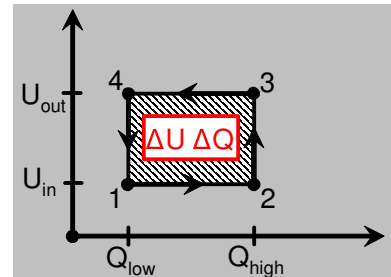


C. Keplinger, A. Koh, S. Bauer, and Z. Suo, „Method for Evaluation, Optimization and Design of Dielectric Elastomer Materials as Actuators and Generators”, manuscript in preparation.



Outlook

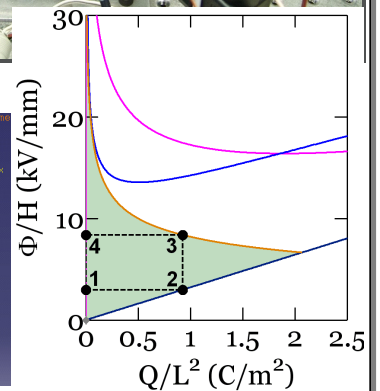
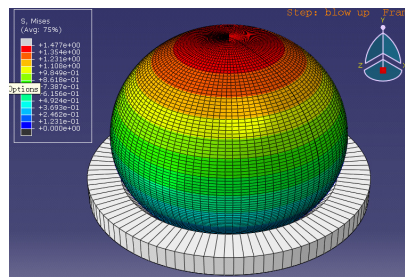
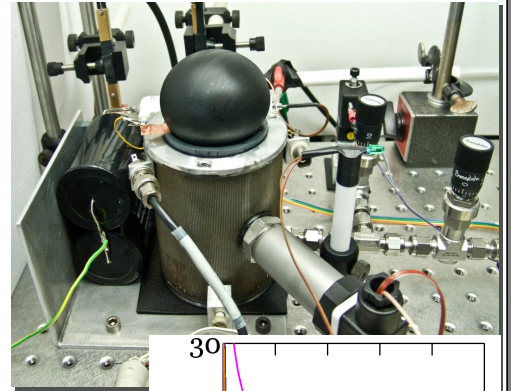
- different cycles, with larger energy of conversion
- different materials
- dynamics → power density
- efficiency, electrical and viscoelastic losses
- scalability, durability (fatigue, imperfections)





Summary

- fully **PC controlled experimental setup** with biaxial and inhomogeneous deformation modes
- combination of **theoretical and exp.** investigations
 - improve basic understanding
 - experiment: well defined thermodyn. cycle, operates between two charge reservoirs
- modeling results will predict optimal operation conditions**
 - maximal energy of conversion for 3MTMVHBTM4910





The Team



Thank you for your attention!

Röntgen's electrode-free elastomer actuators without electromechanical pull-in instability

Christoph Keplinger¹, Martin Kaltenbrunner, Nikita Arnold, and Siegfried Bauer

Soft-Matter Physics, Johannes Kepler University, Altenbergerstrasse 69, A-4040 Linz, Austria

Communicated by Howard Reiss, University of California, Los Angeles, CA, December 15, 2009 (received for review July 23, 2009).

Electrical actuators made from films of dielectric elastomers coated on both sides with stretchable electrodes may potentially be applied in microrobotics, tactile and haptic interfaces, as well as in adaptive optical elements. Such actuators with compliant electrodes are sensitive to the pull-in electromechanical instability, limiting operational voltages and attainable deformations. Electrode-free actuators driven by sprayed-on electrical charges were first studied by Röntgen in 1880. They withstand much higher voltages and deformations and allow for electrically clamped (charge-controlled) thermodynamic states preventing electromechanical instabilities. The absence of electrodes allows for direct optical monitoring of the actuated elastomer, as well as for designing new 3D actuator configurations and adaptive optical elements.

electroactive polymers | dielectric materials | dielectric breakdown | adaptive optics | Maxwell stress

Dielectric elastomer actuators (DEAs) consist of synthetic elastomer films sandwiched between compliant electrodes. For operation, the actuators are connected to a driving voltage source. They emerged as one of the most promising technologies for soft matter–based electromechanical transduction since their discovery by researchers from Stanford Research Institute (1). Coulomb forces between the electrodes squeeze the elastomer in the thickness direction and cause the incompressible elastomer to expand in area. Such “deformable capacitor” designs have shown a cornucopia of potential applications, such as artificial muscles (2) and other bionic applications (3), complex minimum-energy actuators with three-dimensional movements (4–7), energy harvesters (8, 9), adaptive optical elements (10), etc.; commercially available adaptive optical elements are described, for example, at <http://www.optotune.com>. Deformable capacitors are always sensitive to the electromechanical pull-in instability (11–14), which has been first reported to limit the apparent breakdown voltage of soft materials (15), and which has been beautifully demonstrated with closely spaced soap films, which easily deflect measurably under high voltages (16). When the elastomer actuator is subject to a voltage, the elastomer thins down. Thereby, the same voltage induces an increasing electric field in the elastomer and so an increasing attractive force between the oppositely charged electrodes. At the pull-in voltage, this positive feedback causes the elastomer to thin down drastically, finally resulting in electrical breakdown. The pull-in instability is prevented when the elastomer actuator is operated in a charge-controlled mode, because in this case no positive feedback mechanism increases the electric field in the elastomer.

Electrical deformation of solid materials was observed shortly after the invention of the Leyden jar by Fontana, as noted by Volta (17). Such electrical changes in the volume of the Leyden jar were the subject of intense investigations in the late 19th century. Quincke, for example, experimented with Leyden jars made from natural caoutchouc and reported electrically induced volume changes of the jar, which he ascribed to a volume increase of the caoutchouc, roughly proportional to the square of the potential difference between the inner and outer surface of the jar (18). Röntgen criticized Quincke's findings and introduced a simple experiment that illustrates the electrical deforma-

tion of a stretchable body (19). Röntgen used a 16-cm-wide and 100-cm-long stripe of natural rubber, prestretched by a weight to twice its initial length. Upon electrification with sprayed-on electric charges, he was able to observe length changes on the order of several centimeters.

Repeating the experiment of Röntgen with today's materials not only provides an elegant experiment for visualizing the large electrostatic deformations attainable in soft matter, it also allows electrically clamped (charge-controlled) thermodynamic states that are otherwise impossible to access with electrode-coated, electrically free operating actuators (voltage-controlled; originally the term “electrically free” was defined for crystals where the electric field E was dictated by the applied voltage due to a nearly constant thickness; this is not fully valid for soft materials, but it is conventional to use the term in conjunction with “electrically clamped”). Thereby, pull-in instabilities are prevented, giving a nearly unlimited actuation range for actuators (only restricted by the materials breakdown strength). Electrode-free actuator operation will be illustrated with a bending minimum-energy elastomer actuator and a tunable optical lens.

Results

Experimental Analysis of Electrode-Free Elastomer Actuators. The experimental setup for a quantitative analysis of the Röntgen experiment is shown schematically in Fig. 1 and as a photo sequence in Fig. 2. The framework uses an optical rail system where a charging unit is able to move up and down along the elastomer. The charging unit contains two opposed combs of needle electrodes with a separation of 3 cm. Additionally, two opposed Trek Kelvin probe heads are mounted below the needles to enable surface potential measurements on the two surfaces of the elastomer, as illustrated in Fig. S1. Between the optical rails a guideway is placed to pilot an expanding elastomer strip prestretched by the attached mass. Details of the experimental procedure and measurement techniques are described in *Materials and Methods* and in *SI Text*. Three charging cycles at each of the corona voltages of 14, 17, 20, and 23 kV between the two needle setups were initially used, giving stretch ratios up to 1.15, as depicted in Fig. 3. By additionally employing three more charging cycles at 23 kV, a stretch ratio exceeding 1.2 has been achieved. These experimental results reveal a drop of the surface potential difference with increasing deformation after passing a maximum of about 17 kV. This value would be the ultimate limit for conventional voltage-controlled actuators because it would be followed by the pull-in electromechanical instability destroying the actuator. Here, however, the electrically clamped operation enables further deformation and stable states beyond the limits of pull-in. The set of data with the highest stretch ratio has more charges on the elastomer

Author contributions: S.B. designed research; C.K. and M.K. performed research and analyzed data; N.A. and S.B. wrote the paper; and N.A. developed theory.

The authors declare no conflict of interest.

Freely available online through the PNAS open access option.

¹To whom correspondence should be addressed. E-mail: christoph.keplinger@jku.at.

This article contains supporting information online at www.pnas.org/cgi/content/full/0913461107/DCSupplemental.

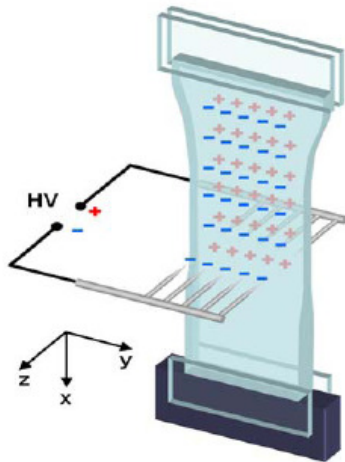


Fig. 1. Linear elastomer actuator geometry pioneered by W.C. Röntgen in 1880. Charges are sprayed on the elastomer by needle combs under high voltage.

than the set with the stretch ratio 1.15, although the voltage is smaller. This results from the thinning of the elastomer (accompanied by the increase in its area); thereby, more charges on the elastomer result in voltages lower than the pull-in value (illustrated in Fig. S2). Breakdown fields of elastomers are usually measured with attached electrodes and are therefore limited by the pull-in instability (16). Materials-related breakdown fields are significantly larger, because our experiments show that stable states beyond pull-in are experimentally accessible. In the subsequent theoretical part, these experimental results are analyzed based on thermodynamic modeling.

To illustrate the extreme deformations achievable by spraying charges onto the surfaces of an elastomer, we prestretched a square piece (5×5 cm) of the tape to a rigid, circular frame with a diameter of 10.4 cm (Fig. 4). Two needle electrodes were placed near the surfaces of the elastomer, and a circular area in the center of the frame was marked with a ballpoint pen to make small deformations visible. To produce the image sequences in Fig. 4, corona voltages of 0, 10, 15, and 25 kV were used from *A* to *D*. From *A* to *B*, the marked ring expands visibly. In *C* regular sinusoidal wrinkles appear, and in *D* the wrinkles become irregular. It is obvious that state *D* can only be realized with an extremely

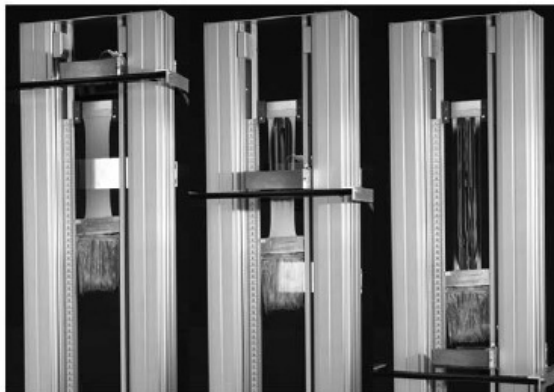


Fig. 2. The image sequence shows the expansion of the elastomer as a result of gradual charging starting at the top. The charging voltage used to produce the pictures was 25 kV.

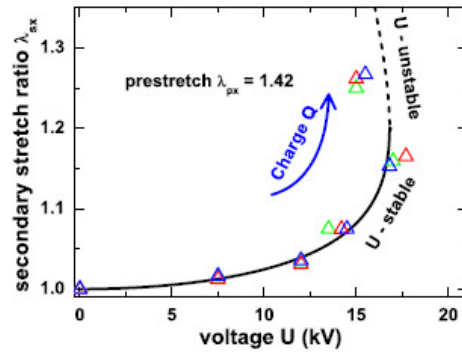


Fig. 3. Secondary stretch λ_{sx} resulting from an incremental increase of the surface charge Q versus the potential difference measured with Kelvin probes on both sides of the elastomer stripe. The colored triangles are sets of data measured in different trials. The solid and dashed curve corresponds to a fit by the second equation of Eq. 8 as explained in the text. Under voltage-controlled, electrically free conditions only the solid line corresponds to stable states limited by the pull-in electromechanical instability. Charge-controlled, electrically clamped conditions stabilize the equilibria even beyond the pull-in limitation.

deformed elastomer. After removal of the corona, the wrinkles disappear, and the initial configuration similar to *A* is restored over several minutes. The experiment is visualized with a video file *Movie S1* provided in *SI Text*. In this video, a moderate voltage with the opposite polarity is used for discharging, and the relaxation takes only a few seconds.

Fig. 5 shows the operation of an electrode-free minimum-energy bending actuator with large actuation range. In the bending actuator, a prestretched elastomer is glued on a flexible frame. Upon release, the actuator bends by minimizing the total free energy consisting of the bending energy of the frame (which

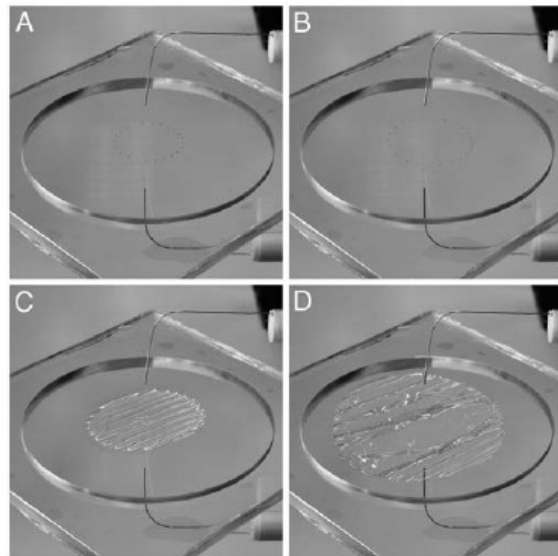


Fig. 4. Radially prestretched elastomer on a rigid frame of 52-mm radius, charged by corona discharge from two needle electrodes. As the corona voltage increases from 0 V in *A* up to approximately 25 kV in *D*, the elastomer first thins and expands in lateral directions as indicated by an ink dot ring (*B*). Regular wrinkles appear in *C*, and finally extreme irregular deformations become possible (*D*). After the removal of corona discharge, the wrinkles disappear, and the initial configuration similar to *A* is restored.

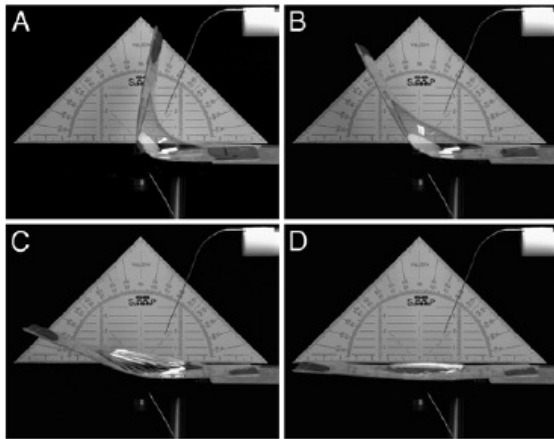


Fig. 5. Photo sequence of an electrode-free minimum-energy bending actuator with large actuation range. As the corona voltage increases from 0 V in *A* up to approximately 20 kV in *D*, the elastomer thins and expands laterally. After removal of the corona discharge, the initial configuration (*A*) is restored.

increases with increase in the bending angle) and the stored elastic energy of the prestretched elastomer (which decreases with bending angle as this decreases elastomer deformation) (5, 6). For the bending actuator to work, it is sufficient to place two needle electrodes near the surfaces. In this case, electrostatic energy adds to the total energy of the elastomer, which makes its decrease with the bending angle less pronounced (5). Therefore, the equilibrium bending angle decreases with the applied voltage. In the image sequences in Fig. 5, we placed a goniometer behind the actuator to demonstrate the large actuation angle of the DEA. The corona voltage is increased from 0 V in *A* to 14 kV in *B*, to 17 kV in *C*, and to 20 kV in *D*. If the voltage is reset to 0 V, the actuator returns to state *A* in a few seconds, which can be accelerated by applying a moderate voltage of the opposite sign (see video file *Movie S2* in *SI Text*). From Fig. 5 it is evident that the total actuation angle is about 100°. The speed of the bending operation is currently limited by our unipolar voltage source, which prevents fast switching from positive to negative voltages. We expect the operation frequency of the actuators to be limited to a few hertz, sufficient for most of the anticipated applications of such actuators.

Fig. 6 shows a sketch of an adaptive lens with variable focal length and aperture, and two photos of the device. In the charged state (Fig. 6 *Right*) the lens thins down, thereby increasing the focal length from its initial value of 210 to 266 mm with a corona voltage of 15 kV. The focal length has been obtained from the known object distance and magnification. The lens is formed by a water drop encapsulated between two elastomer layers. In the images of the device also shown in Fig. 6, the voltage of the corona needles is increased from 0 V (Fig. 6 *Left*) to 15 kV (Fig. 6 *Right*). When the voltage is removed, the lens returns to its initial state in a few seconds. This process is accelerated by applying moderate voltage of opposite sign to the needle electrodes. The two images reveal the increase of both aperture and focal length of the lens when actuated.

Thermodynamic Modeling. The experimental results shown in Fig. 3 are now analyzed in terms of a rigorous thermodynamic model. From the theoretical point of view, our approach to the linear actuator setup proposed by Röntgen is similar to that of Zhao and Suo (12). There exist, however, several differences of various importance. We have chosen to use natural physical variables, such as voltage U and charge Q , rather than nominal electric field

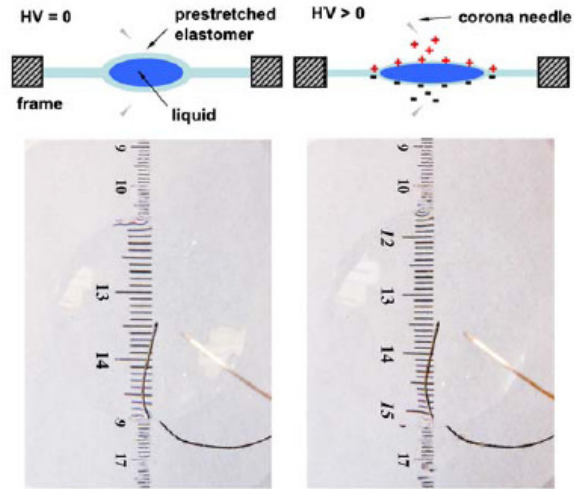


Fig. 6. Adjustable lens with variable focal length and aperture. A drop of water is enclosed between two layers of elastomer. As the corona voltage increases from 0 V (*Left*) up to high voltage (HV) of approximately 15 kV (*Right*), both the aperture and the focal length increase because of the attraction between the elastomer layers.

and displacement that are proportional to them. Furthermore, even when talking about voltage-controlled systems, we do not consider charge as a separate variable. Rather, we consider it as a “fast variable,” which “instantaneously” relaxes to its equilibrium value dictated by the applied voltage. In reality, this happens over the resistor-capacitor (RC) time constant of the system, which is much faster than the time scale of mechanical deformations. With given voltage or charge, the number of variables is reduced to two stretch ratios only, which facilitates modeling. In the subsequent analysis, we proceed analytically as far as possible, mainly by using equilibrium conditions before and after corona charging.

Let the initial dimensions of the elastomer be $x_i, y_i,$ and z_i before the application of a weight with mass m , and $x_p, y_p,$ and z_p after that (subscript p stands for prestretch) (an illustration can be found in Fig. S3). Both sets of dimensions can be measured, but the transition from the i to the p state occurs over a long time scale and is partly viscoelastic. Therefore, i is not the reference state for the prestretch in fast measurements with sprayed-on charges. True prestretch takes place from the auxiliary state 0, which is observed experimentally when the weight is removed from the uncharged elastomer to let it relax on the fast time scale, retaining only the viscoelastic deformation. This is experimentally challenging, and the dimensions $x_0, y_0,$ and z_0 were not measured directly.

For this reason, we use 0 rather than i as the initial reference state in the general development of the theory, but the measurable p state for the definitions of physical parameters, such as capacitance or deformation. The true prestretch $\lambda_{px} \equiv x_p/x_0$ and similar ratios are important, as they define elastic energy. We deduce them from indirect measurements as discussed below. To refer the deformation to the state p , we explicitly separate the overall stretch $\lambda_x \equiv x/x_0$ into a prestretch and a secondary stretch (subscript s) $\lambda_{sx} \equiv x/x_p$, so that $\lambda_x = \lambda_{px}\lambda_{sx}$ for all dimensions $x, y,$ and z . Of course, all derivations can be done equivalently in terms of λ_x only, as was done in ref. 12.

We use the neo-Hookean expression $\frac{G}{2}(\lambda_x^2 + \lambda_y^2 + \lambda_z^2 - 3)$ for the elastic energy density (21). As we factor out the viscoelastic part of the prestretch, the shear modulus G here is the fast one. Because of volume conservation, $V = xyz = x_p y_p z_p = x_0 y_0 z_0$ and $\lambda_x \lambda_y \lambda_z = \lambda_{px} \lambda_{py} \lambda_{pz} = \lambda_{sx} \lambda_{sy} \lambda_{sz} = 1$. The Poisson ratio of most

elastomers is close to 0.5 (20); for the 3M™ VHB™ tape used, the manufacturer claims at least 0.49; literature values have indicated a Poisson ratio of 0.499 (21). However, deviations from incompressible conditions can be taken into account when necessary by modifying the hyperelasticity function. Volume conservation allows us to eliminate all z stretch ratios. We express the gravitational energy of the attached weight using the stretch ratio with respect to the p state: $-mgx = -mgx_p \lambda_{xx}$. The mass m here includes also half of the mass of the elastomer itself, which is usually small. Then, the (free) energy of the uncharged elastomer can be written as

$$F = \frac{GV}{2} (\lambda_{px}^2 \lambda_{xx}^2 + \lambda_{py}^2 \lambda_{yy}^2 + \lambda_{px}^{-2} \lambda_{xx}^{-2} \lambda_{py}^{-2} \lambda_{yy}^{-2} - 3) - mgx_p \lambda_{xx}. \quad [1]$$

Because of viscoelastic effects, we cannot take the prestretch ratios $\lambda_{px,py}$ directly from the experiment, but they should minimize the free energy at the equilibrium p state. Namely, the minimum as a function of λ_{xx} and λ_{yy} should be achieved at values $\lambda_{xx} = \lambda_{yy} = 1$. This results in

$$\begin{aligned} \left. \frac{\partial F}{\partial \lambda_{xx}} \right|_{\lambda_x, \lambda_y=1} = 0 &\Rightarrow GV(\lambda_{px}^2 - \lambda_{px}^{-2} \lambda_{py}^{-2}) = mgx_p \\ \left. \frac{\partial F}{\partial \lambda_{yy}} \right|_{\lambda_x, \lambda_y=1} = 0 &\Rightarrow \lambda_{py}^2 = \lambda_{px}^{-2}. \end{aligned} \quad [2]$$

The first expression relates the prestretch to the applied weight and elastic properties of the material. The second expression merely signifies that the elastomer is uniaxially prestretched.

Electrostatic Energy. The derivation of the electrostatic energy is discussed in detail in *SI Text*, because elastomers with sprayed-on charges differ significantly from electrode-loaded capacitors. Charges need not be symmetrical on both sides, so a careful analysis of the electrostatic problem is required. From experiments we found that the voltage is about constant in the long (x) direction and approximately parabolic in the y direction, with a maximum value U in the middle and half of this value, $U/2$, at the edge. This results in an electrostatic energy:

$$\begin{aligned} W &= -\frac{\epsilon_0 \epsilon_{xy} U^2}{2z} \int_0^1 \underbrace{\left(1 - \frac{y'^2}{2}\right)^2 dy'}_{A \approx 43/60} = -\frac{A \epsilon_0 \epsilon_{xy} U^2}{2z_p} \lambda_{xx}^2 \lambda_{yy}^2 \\ &= -\frac{C_p U^2}{2} \lambda_{xx}^2 \lambda_{yy}^2. \end{aligned} \quad [3]$$

Here, C_p (or more accurately C_p/A) has the meaning of the elastomer capacitance before the start of corona charging. The coefficient A is related to the inhomogeneity in voltage, or, more generally, of thickness and dielectric constant as well. In practice, C_p is used as a fitting parameter within an admissible range.

For the charge-controlled case, the overall charge on each surface stays constant. To keep the similarity with conventional capacitors, we consider half of the total charge difference between the surfaces, Q . It is related to the voltage via

$$Q = \int \frac{\epsilon_0 \epsilon U}{z} dS = \frac{\epsilon_0 \epsilon U xy}{z} \int_0^1 \underbrace{\left(1 - \frac{y'^2}{2}\right) dy'}_{A \approx 5/6} = \frac{\epsilon_0 \epsilon A' U xy}{z}. \quad [4]$$

The energy can be written as the first expression in Eq. 3 (with the opposite sign, because the system is closed and the external source does not perform any work), but one has to group together the terms that stay constant upon deformation: $\frac{A \epsilon_0 \epsilon xy}{2z} U^2 = \frac{A \epsilon_0 \epsilon xy}{2z} \underbrace{\left(\frac{xy}{z} U\right)^2}_{\propto Q^2 = \text{const}}$. The expression in brackets stays constant during the minimization of energy, but the total charge

changes from measurement to measurement, together with the measured voltage. If we exclude z stretch, this can be expressed as follows:

$$W = \frac{C_p U^2 \{\lambda_{xx}^4 \lambda_{yy}^4\}}{2 \lambda_{xx}^2 \lambda_{yy}^2}. \quad [5]$$

Here, U^2 and the combination $\{\lambda_{xx}^4 \lambda_{yy}^4\}$ in braces originate from the constant charge and should not be differentiated when we search for the equilibrium or study its stability. However, λ_{xx} and λ_{yy} should be treated as variables when we resolve the resulting equations to find the actual stretch values as a function of measured voltage U or other parameters.

Using the equilibrium relations in Eq. 2, we can now exclude λ_{py} and either mgx_p or the product GV from the elastic energy expression in Eq. 1. For brevity, we also omit the constant -3 term. Together with the charge-controlled electrostatic contribution from Eq. 5, this results in the following total free energy:

$$\begin{aligned} F &= \frac{GV \lambda_{px}^2}{2} [(\lambda_{xx}^2 - 2\lambda_{xx}) + \lambda_{px}^{-3} (\lambda_{yy}^2 + \lambda_{xx}^{-2} \lambda_{yy}^{-2} + 2\lambda_{xx})] \\ &\quad + \frac{C_p U^2 \{\lambda_{xx}^4 \lambda_{yy}^4\}}{2 \lambda_{xx}^2 \lambda_{yy}^2}. \end{aligned} \quad [6]$$

The consideration of the voltage-controlled case in Eq. 3 is similar. We pulled λ_{px}^2 out of the square brackets to show how it influences the elastic energy. The leading terms in the square brackets are then related to the measurable secondary stretch ratio λ_{xx} . Using the equality $GV(\lambda_{px}^2 - \lambda_{px}^{-1}) = mgx_p$, which follows from Eq. 2, one can replace $GV \lambda_{px}^2 \leftrightarrow \frac{mgx_p}{1 - \lambda_{px}^{-1}}$. The choice between these two expressions is that of more physical fitting. The expression with the mass relies only on the quantities that are directly measured. But in both cases we have to find λ_{px} , which cannot be directly measured because of viscoelastic effects.

The equilibrium condition for the energy expression in Eq. 6 corresponds to its minimum with respect to λ_{xx} and λ_{yy} :

$$\begin{aligned} \frac{\partial F}{\partial \lambda_{xx}} = 0 &\Rightarrow GV \lambda_{px}^2 (\lambda_{xx} - 1 + \lambda_{px}^{-3} (1 - \lambda_{xx}^{-2} \lambda_{yy}^{-2})) = C_p U^2 \lambda_{xx} \lambda_{yy}^2 \\ \frac{\partial F}{\partial \lambda_{yy}} = 0 &\Rightarrow GV \lambda_{px}^{-1} (1 - \lambda_{xx}^{-2} \lambda_{yy}^{-4}) \lambda_{yy} = C_p U^2 \lambda_{xx}^2 \lambda_{yy}. \end{aligned} \quad [7]$$

By dividing these equations onto each other one can express λ_{yy} via λ_{xx} in equilibrium and then write the transcendental equation for λ_{xx} :

$$\begin{aligned} \lambda_{yy}^2 &= \lambda_{xx} [1 + \lambda_{px}^3 (\lambda_{xx} - 1)] \\ \lambda_{xx}^2 [1 + \lambda_{px}^3 (\lambda_{xx} - 1)] &= \left(1 - \frac{\lambda_{xx}^2}{\Lambda^2}\right)^{-1/2}. \end{aligned} \quad [8]$$

Here, we introduced the dimensionless combination $\Lambda^2 = \frac{GV}{C_p U^2 \lambda_{px}^2} \equiv \frac{mgx_p}{C_p U^2 (\lambda_{px}^2 - 1)}$. It characterizes the ratio of the elastic and electrostatic energies, and Λ is inversely proportional to the applied voltage. It is worth noting that it does not depend on the measured x_p value (because C_p is proportional to it). Let us first consider the small voltage (large Λ) behavior. Taylor expansion with small secondary strains $\delta_{\alpha, \beta} \equiv \lambda_{\alpha, \beta} - 1 \ll 1$ results in

$$\delta_{xx} \approx \frac{1}{2\Lambda^2 (\lambda_{px}^3 + 2)} \propto U^2, \quad \delta_{yy} \approx \frac{\lambda_{px}^3 + 1}{2} \delta_{xx}. \quad [9]$$

This implies that the increases in both stretch ratios are proportional to the voltage squared, which can be seen in Fig. 3. The ratio of these increases (which can be measured) defines the real nonviscoelastic prestretch λ_{px} . More accurately, it can be found from the fitting of the first equation of Eq. 8 over a broad range of voltages. From the fit, a value of $\lambda_{px} = 1.42$ (for an initially

50-mm-wide elastomer tape) is obtained. The quality of the fitting is documented in Fig. S4. The last experimental point lies in the wrinkling regime, and the true extension λ_{yy} is actually higher, making the agreement even better. From the physical point of view, the λ_{px} value should lie between 1 and the ratio $x_p/x_i \sim 3$. Another way to actually measure λ_{px} is to let the uncharged elastomer relax without weight to the 0 state on the fast time scale. This results in a prestretch ratio $\lambda_{px} = x_p/x_0 \sim 1.5$ to 1.6, which is a reasonable agreement. This method is less accurate however, due to difficulties of exactly defining the fast time scale. When λ_{px} is determined, the dependence of secondary stretch on the applied voltage, $\lambda_{xx}(U)$, should be found from the solution of the second transcendental equation in Eq. 8. This is done in Fig. 3, which shows two branches of equilibrium solutions as a function of measured voltage. The overall charge increases along the curve as shown by the arrow. The fitting parameter $C_p = 533$ pF used for the calculated curves is in reasonable agreement with typical material values ($\epsilon \approx 4.2$) and measured dimensions of the p state given in *Materials and Methods*.

Voltage-Controlled Case. It is easy to verify, that the equilibrium conditions in Eq. 7 are identical for the voltage-controlled case with the electrostatic energy from Eq. 3. Thus, both cases have the same dependence of equilibrium secondary stretch on measured voltage. This is understandable, because elastic and electrostatic forces are fully determined by the geometry and therefore balance each other in equilibrium at equal values of variables. This argument does not, however, extend to the overall behavior of energy in both systems. In particular, the number of extrema for fixed controlled parameters, as well as their stability [determined by the Hessian of the free energy with respect to λ_{xx} and λ_{yy} (12)] is not the same in both cases. Straightforward, though a bit tedious, calculations show that the charge-controlled case always has a single stable equilibrium, whereas the voltage-controlled case has one minimum and one (unstable) saddle point. The latter becomes stable in the charge-controlled case and corresponds exactly to the upper branch of solutions shown by the dashed curve in Fig. 3. This is in full agreement with the general results of Zhao and Suo (12). In fact, our results based on 2D Hessians are identical with those of Zhao and Suo where 3D Hessians were used. All this can be generalized to arbitrary Legendre-conjugate systems, which will be considered elsewhere.

Discussion

We studied experimentally and analyzed theoretically electrode-free DEAs first suggested by Röntgen (see the historical discussion in Figs. S5 and S6). In this setup, charges from a corona discharge are sprayed on both sides of an elastomer. The problem of electrode degradation and cracking upon stretching is thereby removed. The absence of electrodes and the trapping of charges on the surface allow the system to withstand much higher voltages and electric fields without a global breakdown that disrupts device operation. This allows one to achieve much higher deformations and try out complex 3D geometries with large actuation range, leading to new actuator designs.

Conducting electrodes are inherently equipotential. A free flow of charges along conducting electrodes automatically leads to their concentration near the edges and (if present) corners and

protrusions of the structure. In contrast, deposition of charges at desired positions can be performed dynamically and quite inhomogeneously (22). This permits one (in principle) to achieve a much wider scope of electrostatic contributions to the DEA energetics, which may become especially important for complex 3D geometries. In particular, trapped charges (which do not redistribute freely toward the edges of equipotential surfaces) may contribute to additional lateral Maxwell stresses and larger deformations.

The elastomer without electrodes is transparent and can be monitored using optical techniques. In addition, it can be used to build adaptive optical elements; as an example, we demonstrated lenses with variable focus and aperture based on the Röntgen setup.

From the theoretical point of view, such a setup represents a charge-controlled case, disconnected from the external source, with thermodynamics and energetics different from that of conventional DEAs. States with extreme deformations, which are unstable when the electrodes are present, are stabilized and become accessible for experimental observations. This can be used for materials testing and characterization under severe conditions essential for a safe operation of DEAs. Additional lateral stresses and global potential energy terms may appear because of the trapping of charges on the elastomer surface. This has been addressed mathematically.

By comparing stretches in both lateral directions, we were able to factor out viscoelastic effects and achieve a theoretical description that is virtually free of fitting parameters. Further work may go toward lowering the voltage and miniaturization of the system (for example, using thinner elastomers and carbon-nanotube field emitters) and toward deeper analysis of 3D configurations, including wrinkling.

Materials and Methods

The elastomer samples used for the measurements in corona-charging experiments were 100-mm-long, 50-mm-wide, and 1-mm-thick stripes of a 3M™ VHB™ 4910 acrylic elastomer tape. Upon loading with a weight of mass $m = 150$ g, they typically expand within 24 h to $310 \times 28 \times 0.576$ mm. The relaxation time of 24 h allows the viscoelastic drift of the VHB™ elastomer tape to level off. The following experiments occur on short time scales (minutes) where viscoelastic effects can be ruled out.

The corona needles were connected to a dc high-voltage power supply (model HCL 140-35000, provided by Fu.G. Elektronik GmbH). To maximize the homogeneity of the surface charge distribution in the vertical direction, we moved the charging unit up and down slowly (one cycle ~ 30 s). Reproducibility has been checked by three independent measurement sets.

The surface potential difference has been determined with a Trek Model 341A electrostatic voltmeter based on the Kelvin probe technique. (Further information about the Kelvin probe technique and the setup is given in *SI Text*.) The surface potential along and across the elastomer stripe was recorded on the two surfaces after each cycle. The potential distribution was reproducible with a maximum in the middle of the lateral direction dropping to approximately half the maximum value at the borders. In the vertical dimension, the potential difference was found to be constant within experimental error. The voltage depicted in Fig. 3 refers to the maximum potential difference in the middle of the elastomer stripe.

The elastomer used for the experiments depicted in Fig. 4 and applications shown in Figs. 5 and 6 was the same as in corona-charging experiments.

ACKNOWLEDGMENTS. The work was partially supported by the Austrian Science Fund under Grant P20971-N20.

- Pelrine R, Kombluh R, Pei Q, Joseph J (2000) High-speed electrically actuated elastomers with strain greater than 100%. *Science* 287:836–839.
- Carpi F, De Rossi D, Kombluh R, Pelrine R, Sommer-Larsen P (2008) *Dielectric Elastomers as Electromechanical Transducers: Fundamentals, Materials, Devices, Models and Applications of an Emerging Electroactive Polymer Technology* (Elsevier, Oxford, UK).
- Bar-Cohen Y, David Hanson (2009) *The Coming Robot Revolution: Expectations and Fears About Emerging Intelligent, Humanlike Machines* (Springer, New York).
- Kofod G, Paajanen M, Bauer S (2006) Self-organized minimum-energy structures for dielectric elastomer actuators. *Appl Phys A: Mater Sci Process* 85:141–143.
- Kofod G, Wirges W, Paajanen M, Bauer S (2007) Energy minimization for self-organized structure formation and actuation. *Appl Phys Lett* 90:081916.
- O'Brien B, McKay T, Calius E, Xie SN, Anderson I (2009) Finite element modelling of dielectric elastomer minimum energy structures. *Appl Phys A: Mater Sci Process* 94:507–514.
- Zhao X, Suo Z (2008) Method to analyze programmable deformation of dielectric elastomer layers. *Appl Phys Lett* 93:251902.
- Pelrine R, et al. (2001) Dielectric elastomers: Generator mode fundamentals and applications. *Proc SPIE Int Soc Opt Eng* 4329:148–156.
- Koh A, Zhao X, Suo Z (2009) Maximal energy that can be converted by a dielectric elastomer generator. *Appl Phys Lett* 94:262902.

10. Aschwanden M, Stemmer A (2006) Polymeric, electrically tunable diffraction grating based on artificial muscles. *Opt Lett* 31:2610–2612.
11. Piante JS, Dubowsky S (2006) Large-scale failure modes of dielectric elastomer actuators. *Int J Solids Struct* 43:7727–7751.
12. Zhao X, Suo Z (2007) Method to analyze electromechanical stability of dielectric elastomers. *Appl Phys Lett* 91:061921.
13. Zhao X, Hong W, Suo Z (2007) Electromechanical coexistent states and hysteresis in dielectric elastomers. *Phys Rev B: Condens Matter Mater Phys* 76:134113.
14. Keplinger C, Kaltenbrunner M, Arnold N, Bauer S (2008) Capacitive extensometry for transient strain analysis of dielectric elastomer actuators. *Appl Phys Lett* 92:192903.
15. Stark KH, Garton CG (1955) Electric strength of irradiated polythene. *Nature* 176:1225–1226.
16. Taylor G (1968) The coalescence of closely spaced drops when they are at different electric potentials. *Proc R Soc Lond A* 306:423–434.
17. Volta A Lettere Inedite di Alessandro Volta scritto dal professore Pietro Gonfigliacchi (Pesaro stamperia nobili) (Unpublished letters of Alessandro Volta, collected by Pietro Gonfigliacchi).
18. Quincke G (1880) Ueber elektrische Ausdehnung. *Ann Phys Chem* 10:163–553.
19. Röntgen WC (1880) Ueber die durch Electricität bewirkten Form—und Volumenänderungen von dielectrischen Körpern. *Ann Phys Chem* 11:771–786.
20. Treloar LRG (1975) *The Physics of Rubber Elasticity* (Oxford Univ Press, Oxford, UK).
21. Beck MD, Aschwanden M, Belyaev Y, Stemmer A (2006) Tunable optical active elements. European Patent Application EP1826591 Available at <http://www.freepatentonline.com/EP1826591.html>.
22. Jacobs HO, Whitesides GM (2001) Submicrometer Patterning of Charge in Thin-Film Electrets. *Science* 291:1763–1766.

Supporting Information

Keplinger et al. 10.1073/pnas.0913461107

SI Text

Experimental Details. Fig. S1 (*Left*) illustrates the Kelvin probe measurement to obtain the surface potential of the elastomer. The vertical gray stripe depicts the cross section of the elastomer. The blue and yellow squares illustrate the sprayed-on charges, and the electric field is illustrated by small arrows. In addition, equipotential lines are drawn. To assess the surface potential of the elastomer via non-contact measurements, the housing of the probe head (gray rectangle with yellow border) is driven to a potential equal to the surface potential of the elastomer by approximately nulling the electric field in the gap. Fig. S1 (*Right*) shows the experimental arrangement with two Kelvin probes to measure the potentials $\varphi_{1,2}$ on both surfaces of the elastomer; the voltage U between the two elastomer surfaces is then obtained from the potential difference between the two Kelvin probe readings.

In Fig. 3 it seems surprising that the voltage measured at the highest stretch ratio of 1.25 is smaller than the voltage at the lower stretch ratio of 1.15, although there are more charges on the elastomer at a stretch ratio of 1.25 as compared to the stretch ratio of 1.15. Fig. S2 illustrates such a situation. Whereas on the left side, with a thick elastomer the charge Q_1 is smaller than the charge Q_2 , on the right side, with a thinner elastomer and a larger area, the opposite is true for the voltages: U_1 is larger than U_2 .

The geometry for the theoretical modeling is illustrated in Fig. S3. The initial dimensions of the elastomer are denoted with a subscript i ; the dimensions p stand for the prestretched state. The transition from the i to the p state is partly viscoelastic. The reference state 0 can be obtained on a short time scale if the mass m used for prestretching is removed. Stretching to the final state after charging is described from the reference state 0.

Fig. S4 illustrates the excellent fit used to obtain the prestretch parameter $\lambda_{px} = 1.42$, as discussed in the main text.

Experiments shown in Figs. 4 and 5 of the manuscript are illustrated with two video files. In Movie S1 the reversibility of the large deformations of an elastomer surface is demonstrated. Even the huge irregular deformations visible in Fig. 4D fully recover to the initial flat state.

Movie S2 illustrates the operation of the electrode-free bending actuator. The speed of operation is currently limited by the used dc high-voltage power supply. In order to discharge the actuator, the polarity of the supply must be changed. This is only possible by switching the device off, followed by a manual change of polarity.

Theoretical Considerations on Elastomer Stripes with Sprayed-on Charges. An elastomer with sprayed-on electrical charges differs significantly from a deformable electrode coated capacitor. Conducting electrodes are equipotential surfaces, and the free flow of electrons along them concentrates the charges near the edges and corners of the structure. In contrast, elastomers with sprayed-on electrical charges may have charge distributions that are different on the top and bottom surface of the elastomer. In the article we have made the approximation that the energetics of an elastomer with sprayed-on electrical charges is dominated by the usual capacitor term.

In order to verify our approximations, we rigorously solve the problem of a plane dielectric of finite thickness h with arbitrary surface charge densities on both sides. The electrostatic energy can be written in two equivalent forms (1) (centimeter-gram-second Gaussian system is used here): $W = \frac{1}{8\pi} \int \mathbf{E} dV =$

$\frac{1}{2} \int \varphi dq$. The last integral can be over the volume, or surface, or a mixture of both. It is usually simpler than the first expression, especially when the integration should be done only over the surface charges as in our case. To calculate the energy, we solve a Poisson-type equation for the potential φ , $\text{div} \mathbf{D} = -\text{div}(\epsilon \text{grad} \varphi) = 4\pi\rho$ everywhere; find the field $\mathbf{E} = -\nabla\varphi$ and the displacement $\mathbf{D} = \epsilon\mathbf{E}$ and calculate the energy using any of the two aforementioned integrals.

The dielectric will occupy a layer $0 < z < h$, and subscripts 0 and h refer to the corresponding z planes. Subscript e refers to the elastomer. Because only surface charge densities σ are present, the potential satisfies the Laplace equation $\Delta_{\perp}\varphi + \varphi_{zz} = 0$ both inside and outside of the elastomer. Here we mean under Δ_{\perp} the part of the Laplacian in the (x, y) plane $\Delta_{\perp} = \partial_{xx} + \partial_{yy}$. Applying a Fourier transformation in the x - y plane (denoted by tilde, $\tilde{\varphi}$) we get $-k^2\tilde{\varphi} + \tilde{\varphi}_{zz} = 0$ where $k^2 = k_x^2 + k_y^2$ is the square of the Fourier wavevector, and the subscript z denotes differentiation. The solutions of this equation outside and inside the elastomer can be written as

$$\begin{aligned} \tilde{\varphi}_{-} &= c_{-}e^{kz}, & z < 0; & & \tilde{\varphi}_{e} &= c_1e^{kz} + c_2e^{-kz}, & 0 < z < h; \\ \tilde{\varphi}_{+} &= c_{+}e^{-k(z-h)}, & z > h. & & & & \end{aligned} \quad [\text{S1}]$$

With such notations the conditions at infinities are satisfied automatically, and the coefficients c_{\pm} have the meaning of the potentials on both surfaces: $\tilde{\varphi}_0 = c_{-}$, $\tilde{\varphi}_h = c_{+}$. The continuity of the potential and the change in the normal derivative of (Fourier image of) the electric displacement $\tilde{D}_n \equiv (1/\epsilon)\tilde{E}_n \equiv -(1/\epsilon)\tilde{\varphi}_z$ on both surfaces can be written as follows:

$$\begin{aligned} \tilde{\varphi}_{-}(0) &= \tilde{\varphi}_e(0) \Rightarrow c_{-} = c_1 + c_2, \\ \epsilon \frac{d\tilde{\varphi}_e}{dz} \Big|_0 - \frac{d\tilde{\varphi}_{-}}{dz} \Big|_0 + 4\pi\tilde{\sigma}_0 &= 0 \Rightarrow kc_{-} - \epsilon k(c_1 - c_2) = 4\pi\tilde{\sigma}_0, \\ \tilde{\varphi}_{+}(h) &= \tilde{\varphi}_e(h) \Rightarrow c_{+} = c_1e^{kh} + c_2e^{-kh}, \\ \frac{d\tilde{\varphi}_{+}}{dz} \Big|_h - \epsilon \frac{d\tilde{\varphi}_e}{dz} \Big|_h + 4\pi\tilde{\sigma}_h &= 0 \Rightarrow kc_{+} + \epsilon k(c_1e^{kh} - c_2e^{-kh}) = 4\pi\tilde{\sigma}_h. \end{aligned} \quad [\text{S2}]$$

This system of linear equations can be easily solved. Subsequently, we will often use symmetric and asymmetric parts of the charge and potential distributions (or their Fourier transforms), defined as follows:

$$\begin{aligned} \sigma &= \sigma_h + \sigma_0, & \delta &= \sigma_h - \sigma_0, & \text{which implies} & & \sigma_{0,h} &= (\sigma \mp \delta)/2 \\ u &= \varphi_h + \varphi_0, & v &= \varphi_h - \varphi_0, & & & \varphi_{0,h} &= (u \mp v)/2 \end{aligned} \quad [\text{S3}]$$

With these notations, the coefficients c_{\pm} , which are equal to the surface potentials, are found to be

$$c_{\mp} \equiv \tilde{\varphi}_{0,h} = \frac{2\pi}{k} \left(\frac{\tilde{\sigma}}{1 + \epsilon \text{th} \frac{kh}{2}} \mp \frac{\tilde{\delta} \text{th} \frac{kh}{2}}{\epsilon + \text{th} \frac{kh}{2}} \right). \quad [\text{S4}]$$

We use these formulas to relate charge densities and potentials. Their symmetric and asymmetric parts separate and are proportional to each other in Fourier space:

$$\begin{aligned}
\tilde{\sigma} &= \frac{k}{4\pi} \left(1 + \epsilon \operatorname{th} \frac{kh}{2} \right) \tilde{u} \approx \frac{k}{4\pi} \tilde{u} + \underbrace{O(h^2 k \tilde{u})}_{\leq h^2 k \tilde{u}}, \\
\tilde{\delta} &= \frac{k}{4\pi} \frac{\epsilon + \operatorname{th} \frac{kh}{2}}{\operatorname{th} \frac{kh}{2}} \tilde{v} \approx \left(\frac{\epsilon}{2\pi h} + \frac{k}{4\pi} \right) \tilde{v} + \underbrace{O(h^2 k \tilde{v})}_{\sim h^2 k \tilde{v}}, \\
\tilde{u} &= \frac{4\pi}{k} \frac{\tilde{\sigma}}{1 + \epsilon \operatorname{th} \frac{kh}{2}} \approx \frac{4\pi}{k} \tilde{\sigma} + \underbrace{O(h \tilde{\sigma})}_{\sim h k \tilde{\sigma} \leq h k \tilde{v}}, \\
\tilde{v} &= \frac{4\pi}{k} \frac{\tilde{\delta} \operatorname{th} \frac{kh}{2}}{\epsilon + \operatorname{th} \frac{kh}{2}} \approx \left(\frac{2\pi h}{\epsilon} - \frac{\pi h^2 k}{\epsilon^2} \right) \tilde{\delta} + \underbrace{O(h^3 k^2 \tilde{\delta})}_{\sim h^2 k^2 \tilde{v}}.
\end{aligned} \tag{S5}$$

The approximate expressions are Taylor expansions up to the first meaningful order in (small) thickness h . It requires a different number of terms in different formulas, as will become clear from the energy expressions below. There exists subtlety in the comparison between the different terms in the potential and charge representation. If the characteristic in-plane size of the system is a , the important wavevectors are $k \sim 1/a$, and the small parameter in the Taylor expansion is $hk \sim h/a \ll 1$. From the Fourier representation (Eq. S5) we get

$$\frac{\tilde{\sigma}}{\tilde{\delta}} = \frac{1 + \epsilon \operatorname{th} \frac{kh}{2}}{\frac{\epsilon + \operatorname{th} \frac{kh}{2}}{\operatorname{th} \frac{kh}{2}}} \frac{\tilde{u}}{\tilde{v}} \approx \frac{kh \tilde{u}}{2\epsilon \tilde{v}}. \tag{S6}$$

This means that the ratio of the symmetric/asymmetric terms always has a different order of magnitude for charges and potentials. For our experimental conditions it is always small for the charges, but not necessarily small for the potentials. From the experiment, we know that typically $u \leq v$. Correspondingly, $\sigma \leq kh\delta \ll \delta$. As shown below, the symmetric and asymmetric parts separate in the energy expression in the Fourier space (Eq. S13). The coefficient in the asymmetric potential term is a factor of $1/kh$ larger than for the symmetric part. For this reason we make a Taylor expansion up to zero order in the symmetric terms, but up to the first order in asymmetric ones. Orders of magnitude of the errors for the worst realistic case $u \sim v$ are indicated in Eq. S5.

The approximate formulas for small thicknesses can be analytically Fourier-inverted for arbitrary charge densities. The two-dimensional (2D) (direct or inverse) Fourier transform (with symmetric prefactor) has the following properties (2):

$$k^{-2} f = r^{-1}, \quad \tilde{f}^* g = 2\pi \tilde{f} \tilde{g}, \quad \Delta_{\perp}^{-1} f = -k^{-2} \tilde{f}. \tag{S7}$$

Here the asterisks stands for 2D convolution. The inversion of \tilde{k} cannot be done in a similar fashion because of the singularities involved. Using the first two properties, we can obtain a Fourier inversion of the expression

$$\tilde{\varphi}_s = \frac{2\pi}{k} \tilde{\sigma}, \quad \text{which is the single-layer potential} \quad \varphi_s \equiv \sigma * \frac{1}{r}. \tag{S8}$$

The Fourier inversion of the function f in combination with different powers of k can be written as follows:

$$\begin{aligned}
\frac{1}{k} \tilde{\tilde{f}} &= \frac{1}{2\pi r} * f, & \tilde{\tilde{f}} &= f, & k \tilde{\tilde{f}} &= \frac{-1}{k} (\tilde{-k^2 \tilde{f}}) = \frac{-1}{2\pi r} * \Delta_{\perp} f, \\
k^2 \tilde{\tilde{f}} &= -\Delta_{\perp} f.
\end{aligned} \tag{S9}$$

This allows us to invert analytically the small thickness expressions in Eq. S5:

$$\begin{aligned}
\sigma &\approx -\frac{1}{8\pi^2 r} * \Delta_{\perp} u, & \delta &\approx \frac{\epsilon}{2\pi h} v - \frac{1}{8\pi^2 r} * \Delta_{\perp} v, & u &\approx \frac{2}{r} * \sigma, \\
v &\approx \frac{2\pi h}{\epsilon} \delta + \frac{h^2}{2\epsilon^2 r} * \Delta_{\perp} \delta.
\end{aligned} \tag{S10}$$

For the surface potentials in terms of charge densities and vice versa we get

$$\begin{aligned}
\varphi_{0,h} &= \frac{u \mp v}{2} \approx \frac{1}{r} * \sigma \mp \left(\frac{\pi h}{\epsilon} \delta + \frac{h^2}{4\epsilon^2 r} * \Delta_{\perp} \delta \right), \\
\sigma_{0,h} &= \frac{\sigma \mp \delta}{2} \approx -\frac{1}{16\pi^2 r} * \Delta_{\perp} u \mp \left(\frac{\epsilon}{4\pi h} v - \frac{1}{16\pi^2 r} * \Delta_{\perp} v \right) \\
&= -\frac{1}{16\pi^2 r} * \Delta_{\perp} \varphi(0, h) \mp \frac{\epsilon}{4\pi h} v.
\end{aligned} \tag{S11}$$

One can recognize the global potential of the single layer φ_s , the double layer capacitor term, and some addition related to the in-plane inhomogeneity of the double layer in the simplified expressions. Surface charge densities in terms of potentials are given by the contributions from the global term for each surface potential and the asymmetric capacitor contribution.

Total electrostatic energy. It is convenient to calculate the energy in the Fourier space, because then the intermediate results are exact. According to Parseval's theorem (2) (in unitary convention), $\iint g^* dS = \iint \tilde{g}^* dS_k$. Here asterisk superscripts denote complex conjugates. Thus, the energy can also be calculated as the integral of the product of the Fourier images of the charges and potentials. All our functions are real and even with respect to x and y (or can be made even by quadrupling of their domain). Therefore, their Fourier transforms are also real, and we can write for the surface differential of the electrostatic energy:

$$\begin{aligned}
dW &= \frac{\varphi_0 \sigma_0 + \varphi_h \sigma_h}{2} dS = \frac{u\sigma + v\delta}{4} dS \rightarrow \frac{\tilde{\varphi}_0 \tilde{\sigma}_0 + \tilde{\varphi}_h \tilde{\sigma}_h}{2} dS_k \\
&= \frac{\tilde{u} \tilde{\sigma} + \tilde{v} \tilde{\delta}}{4} dS_k.
\end{aligned} \tag{S12}$$

Using the relationships in Eq. S5, this can be written in terms of charges or potentials only, in exact or in approximate form. Symmetric and asymmetric variables $u \propto \sigma$, $v \propto \delta$ separate, and the energy is always diagonal in terms of these variables:

$$\begin{aligned}
dW &= \frac{k}{16\pi} \left(\left(1 + \epsilon \operatorname{th} \frac{kh}{2} \right) \tilde{u}^2 + \frac{\epsilon + \operatorname{th} \frac{kh}{2}}{\operatorname{th} \frac{kh}{2}} \tilde{v}^2 \right) dS_k \\
&= \frac{\pi}{k} \left(\frac{\tilde{\sigma}^2}{1 + \epsilon \operatorname{th} \frac{kh}{2}} + \frac{\tilde{\delta}^2 \operatorname{th} \frac{kh}{2}}{\epsilon + \operatorname{th} \frac{kh}{2}} \right) dS_k \\
&\approx \left(\frac{k \tilde{u}^2}{16\pi} + \frac{\epsilon \tilde{v}^2}{8\pi h} + \frac{k \tilde{v}^2}{16\pi} \right) dS_k \\
&\quad \substack{\leq h^2 & \substack{(kh)^{-1} k^2 \\ \gg h^2} & k^2} \\
&\approx \left(\frac{\pi \tilde{\sigma}^2}{k} + \frac{\pi h \tilde{\delta}^2}{2\epsilon} - \frac{\pi h^2 k \tilde{\delta}^2}{4\epsilon^2} \right) dS_k.
\end{aligned} \tag{S13}$$

Under each term of the Taylor expansion, we indicated the relation to the last term (lowest order correction in v and δ), assuming the worst case $u \sim v$. For $u \ll v$ the terms with u or σ

should be dropped, because omitted terms with v and δ are larger. But we always retain the leading correction in v and δ . The central (capacitor) term is the largest unless $u \gg v$ (almost equal charges on both sides). In this case not all terms in Eq. S13 are meaningful, but the largest term is related to the u or σ expressions (global energy of a single layer). The transition to this regime occurs with $u^2 \sim v^2 a/h$.

Let us transform the approximate energy expression in Eq. S13 written in terms of potentials using the approximate potential-charge relations from Eq. S5. If we retain only the leading terms after squaring, this results in

$$\begin{aligned}
 dW &\approx \left(\underbrace{\frac{k\tilde{u}^2}{16\pi}}_{\leq kv^2} + \underbrace{\frac{\epsilon\tilde{v}^2}{8\pi h}}_{\substack{(h)^{-1}k^2 \\ \gg b^2}} + \underbrace{\frac{k\tilde{v}^2}{16\pi}}_{kv^2} \right) dS_k \\
 &\approx \left(\underbrace{\frac{\pi\tilde{\sigma}^2}{k}}_{\substack{\leq (kh)^2 \delta^2 R \\ \leq (R/h)^2}} + \underbrace{\frac{\pi h \tilde{\delta}^2}{2\epsilon}}_{\substack{h^2 \\ \gg (h)^2}} - \underbrace{\frac{\pi h^2 k \tilde{\delta}^2}{2\epsilon^2}}_{(kh)h\delta^2} + \underbrace{\frac{\pi h^2 k \tilde{\delta}^2}{4\epsilon^2}}_{(kh)h\delta^2} \right) dS_k \\
 &\approx \left(\underbrace{\frac{\pi\tilde{\sigma}^2}{k}}_{\substack{\leq (R/h)^2 \delta^2 R \\ \leq (R/h)^2}} + \underbrace{\frac{\pi h \tilde{\delta}^2}{2\epsilon}}_{\substack{h^2 \\ \gg (h)^2}} - \underbrace{\frac{\pi h^2 k \tilde{\delta}^2}{4\epsilon^2}}_{(kh)h\delta^2} \right) dS_k. \quad \text{[S14]}
 \end{aligned}$$

Therefore, we recover the last expression (Eq. S13) obtained by Taylor expansion of the energy in the charge representation. The global u term related to the single layer potential always transforms directly into the global σ term and vice versa. The global δ term related to the asymmetric charge distribution contains the contribution from the capacitor v term. Conversely, in the transformation from the charge to the potential representation, the capacitor δ term will contribute to both capacitor v and global v terms.

The inversion of the approximate expressions in Eq. S13 can be performed analytically for arbitrary potentials or charge profiles using Parseval's theorem and properties of the Fourier inversion (Eq. S9). We write the capacitor term in front and indicate the order of magnitude of all terms assuming that typical sizes of the elastomer rectangle are a (smaller side) and b (larger side). Remember that $\sigma \sim kh\delta \sim h\delta/a$, and the convolution brings an area integration factor $\sim ab$:

$$\begin{aligned}
 dW &\approx \left(\frac{\epsilon\tilde{v}\tilde{v}}{8\pi h} + \frac{(k\tilde{u})\tilde{u} + (k\tilde{v})\tilde{v}}{16\pi} \right) dS_k \\
 &\rightarrow \left(\frac{\epsilon v^2}{8\pi h} - \frac{(\frac{1}{r} * \Delta_1 u)u + (\frac{1}{r} * \Delta_1 v)v}{32\pi^2} \right) dS, \\
 &\quad \substack{v^2/h \\ (ab/b)(a^2/a^2) \leq v^2/a \\ v^2/a} \\
 dW &\approx \left(\frac{\pi h \tilde{\delta} \tilde{\delta}}{2\epsilon} + \frac{2\pi \tilde{\sigma} \tilde{\sigma}}{k} - \frac{\pi h^2 (k\tilde{\delta})\tilde{\delta}}{4\epsilon^2} \right) dS_k \quad \text{[S15]} \\
 &\rightarrow \left(\frac{\pi \delta^2 h}{\epsilon} + \frac{\overbrace{\left(\frac{1}{r} * \sigma\right)\sigma}^{\varphi_S}}{2} + \frac{h^2 (\frac{1}{r} * \Delta_1 \delta)\delta}{8\epsilon^2} \right) dS. \\
 &\quad \substack{\delta^2 h \\ (ab/b)\sigma^2 \leq \delta^2 h^2/a \\ h^2(ab/b)(\delta^2/a^2) \sim \delta^2 h^2/a}
 \end{aligned}$$

The first term everywhere is the capacitor term. The second term is the global term. As explained above, when one switches between the charge and potential representations, the terms transform into each other in a nontrivial way. Omitted terms

are smaller than at least one of the retained terms. These expressions are not trivial. They involve the integration over the elastomer area and include convolutions and Laplacians. However, orders of magnitude indicated for each term show that for a thin elastomer with $h/a \ll 1$ we can restrict ourselves to the capacitor terms in Eqs. 3 or 5 employed in the main text. Note that there, for practical convenience, we use the International System of Units and the conventional notation U for the asymmetric part of the potential (voltage) v , as defined in Eq. S3.

Although the capacitor term looks deceptively simple, its spatial inhomogeneity accounts for one more subtle and important effect. In plane DEAs with conducting equipotential electrodes, there are no lateral electrostatic forces acting on the elastomer, whereas for nonconducting elastomers with fixed charges they are present and should be reflected in the electrostatic energy. The obtained formulas show that within the approximations made, such forces are taken into account simply by the capacitive energy expression with a variable voltage. Indeed, the potential varies along the surface exactly because the charge distribution is different from that on the equipotential plates of conventional capacitors. The charge distribution might be rather homogeneous in the beginning of the corona spraying cycle. This creates an elevated potential in the center, which deflects subsequently arriving ions toward the edge of the stripe as the charging proceeds. As a result, the final charge density is higher toward the edges, but is not as high as for conducting electrodes. The elevated potential (and voltage) in the middle of the stripe were indeed measured experimentally.

Additional Historical Information. For the interested reader we have copied a few pivotal parts of Quincke's and Röntgen's work in the original German version together with translations in English. In the translation we have tried to keep the initial intent and stylistic flavor of the authors.

Translation of extracts from Quincke's work titled "On electrical expansion" (original German version compiled in Fig. S5) (3):

One will learn from this that solid and liquid isolators change their volume, if they are, similarly to the glass of a Leyden jar, exposed to electrical forces. The volume can increase thereby, what is the most typical, but it can also decrease. The volume change does not originate from electrical compression. The expansion of the glass caused by the electrical forces is homogeneous in all directions, like a thermal expansion, but it does not originate from warming. Simultaneously with the dimensions, also the elastic force of the isolator changes under the influence of the electrical forces. One set of substances shows a decrease here, another set shows an increase.

Thermometer capacitors made of caoutchouc were fabricated in such a way, that in one end of a long, black caoutchouc hose a capillary tube with a fused-in platinum wire was cemented with Shellac and Canada balsam, whereas in the other end a short tube of flint glass was drawn to a needle and similarly fixed.

From these experiments one can learn that the volume increase of caoutchouc is, like it is true for glass and glimmer, almost proportional to the square of the electric potential difference between the capacitor electrodes. Under equal conditions the increase for fresh caoutchouc is ten times higher than for glass; for caoutchouc, which was in contact with water for two days, values are similar to glass.

Translation of extracts from Röntgen's work titled "On the shape- and volume changes of dielectric bodies caused by electricity" (original German version compiled in Fig. S6) (4):

Finally, to those colleagues, who may wish to see an electrical deformation of a solid body without attempting to quantify the process, I would like to recommend the following experiment, which I carried out in 1876, and which I on occasion presented to the assembly of natural scientists in Baden-Baden (1879) among other findings. An approximately 16 cm wide and 100 cm long, rectangular stripe of thin, red caoutchouc is clamped between two small wooden ledges at the top and the bottom; the upper clamp is attached to some kind of arm or hook in such a way, that the caoutchouc stripe hangs freely; the bottom clamp is loaded with weights, which stretch the stripe approximately to the double length. After having waited till the elastic aftereffect has become imperceptible, one observes the position of the bottom end of the stripe, for example on a paper scale placed nearby, while the caoutchouc is electrified by an assistant. For that purpose the assistant holds in each hand an isolated comb of needles, where one of them is connected by a conductor to the positive and the other to the negative electrode of a strong Holtz influence machine; the caoutchouc stripe

hangs between the parallel held combs, but the former is not touched by the needles. As the assistant starts for example at the top and gradually lowers both combs, a larger and larger part of the caoutchouc becomes electrified; accordingly one observes a continuous increase of the length of the band, which finally, when the whole stripe is electrified, amounts to several centimeters. Since dry caoutchouc is a good isolator, this lengthening persists for a long time afterward. It can, however, at least to a large degree, be removed by discharging the stripe, which is done in a similar way to the charging process; but the combs have to be now connected to the ground.

Mr. Quincke has also published (1880) similar experiments and believes that one is allowed to conclude from them, that the elasticity of solid bodies is changed by electrical forces; I, from my side, regard this conclusion as rather daring, and after an assessment of Quincke's experiments I didn't find an inducement to share his opinion; however, since I am worried that this article would get too long, I prefer to refrain from disclosing the motives for my negatory attitude.

1. Landau LD, Lifshitz EM, Pitaevskii LP (1984) *Electrodynamics of Continuous Media* (Pergamon, New York), 2nd Ed., *Course of Theoretical Physics*, Vol. 8.
2. Korn GA, Korn TM (2000) *Mathematical Handbook for Scientists and Engineers: Definitions, Theorems, and Formulas for Reference and Review* (Dover, New York), 2nd Ed.
3. Quincke G (1880) Ueber elektrische Ausdehnung. *Ann Phys Chem* 10:163–203, 374–414, 513–553.
4. Röntgen WC (1880) Ueber die durch Electricität bewirkten Form- und Volumenänderungen von dielectricischen Körpern. *Ann Phys Chem* 11:771–786.

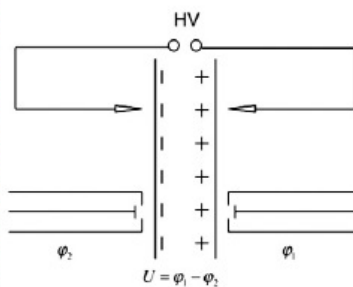
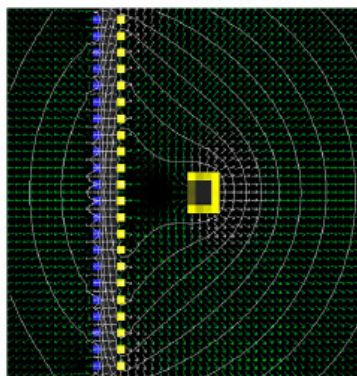


Fig. S1. (Left) Illustration of the Kelvin probe technique for measuring the surface potential. In the Röntgen experiment two Kelvin probes are used to monitor the surface potential on both sides of the film. (Right): Scheme of the experimental setup with two Kelvin probes for measuring the potential on both surfaces of the elastomer.

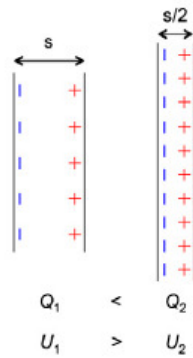


Fig. S2. Schematic illustration of the charges on the elastomer and of the voltages across the elastomer in a thick state with a low stretch ratio and in a thin state with a high stretch ratio, which also has larger area. Whereas the *Left* state can be stable under voltage-controlled conditions, the *Right* state is in the pull-in region. In the charge-controlled operation mode, both states are thermodynamically stable.

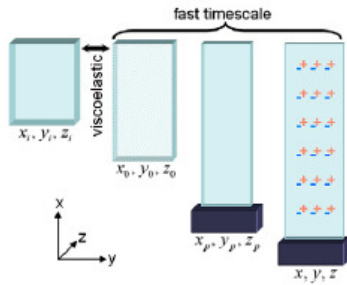


Fig. S3. Illustration of the different deformation dimensions used in the text. The initial state *i* is characterized by the dimensions x_i , y_i , and z_i , and the weight-loaded state *p* has sizes x_p , y_p , and z_p . The transition from the *i* to *p* state takes several hours and is partly viscoelastic. State 0 with dimensions x_0 , y_0 , and z_0 is an auxiliary starting state, which discards viscoelastic effects. The prestretches $\lambda_{px,py,pz}$ characterize the transition from 0 to *p*. The charged state has the dimensions x , y , and z and is characterized by the secondary stretches $\lambda_{sx, sy, sz}$ referred to the *p* state.

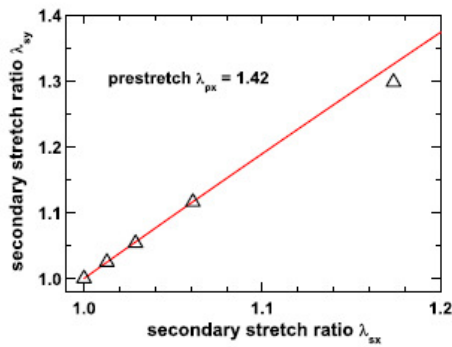


Fig. S4. Relation between the lateral secondary stretches λ_{sy} and λ_{sx} . It allows one to deduce real nonviscoelastic prestretch λ_{px} experimentally. The solid curve, fit with the first equation of Eq. 8, uses a prestretch value of $\lambda_{px} = 1.42$.

Man wird daraus ersehen, dass feste und flüssige Isolatoren ihr Volumen ändern, wenn man sie, ähnlich wie das Glas einer Leydener Flasche, electricischen Kräften aussetzt.

Das Volumen kann dabei vermehrt werden, was das gewöhnlichste ist, oder auch vermindert werden. Die Volumenänderung rührt nicht von electricischer Compression her.

Die von electricischen Kräften hervorgerufene Ausdehnung des Glases erfolgt nach allen Richtungen gleichmässig, wie durch Erwärmung, rührt aber nicht von Erwärmung her.

Gleichzeitig mit den Dimensionen ändert sich auch die elastische Kraft des Isolators unter dem Einflusse der electricischen Kräfte. Bei einer Reihe Substanzen nimmt sie dadurch ab, bei einer andern Reihe zu.

§ 18. Thermometercondensatoren aus Kautschuk wurden in der Weise hergestellt, dass in dem einen Ende eines langen, schwarzen Kautschukschlauchs eine Capillarröhre mit eingeschmolzenem Platindraht, in dem andern Ende ein kurzes, in eine Spitze ausgezogenes Flintglasrohr mit Schellack und Canadabalsam eingekittet wurde.

Aus diesen Versuchen geht hervor, dass die Volumenzunahme des Kautschuks wie bei Glas und Glimmer nahezu proportional ist dem Quadrate der electricischen Potentialdifferenz auf beiden Belegungen des Condensators. Bei sonst gleichen Umständen ist die Zunahme für frischen Kautschuk mehr als zehnmal grösser als bei Glas; für Kautschuk, der zwei Tage mit Wasser in Berührung gewesen, etwa ebenso gross wie bei Glas.

Fig. 55. Extracts from Quincke's original work in German.

Zum Schluss möchte ich denjenigen Fachgenossen, welche vielleicht eine electriche Deformation eines festen Körpers zu sehen wünschen, ohne dieselbe messend verfolgen zu wollen, folgenden Versuch empfehlen, den ich im Jahr 1876 angestellt und bei Gelegenheit der Naturforscherversammlung zu Baden-Baden (1879) unter anderen mitgetheilt habe.¹⁾ Ein ungefähr 16 cm breiter und 100 cm langer, rechteckiger Streifen aus

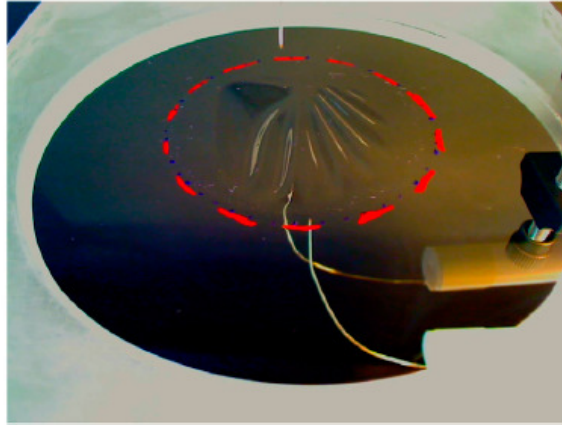
1) Röntgen, Tageblatt der 52. Versammlung, p. 184 1876.
Ann. d. Phys. u. Chem. N. F. XI. 50

dünnem, rothem Kautschuk wird oben und unten zwischen je zwei Holzleisten festgeklemmt; die obere Klemme wird an irgend einem Arm oder Haken so befestigt, dass das Kautschukband frei herunterhängt; an die untere Klemme werden Gewichte gehängt, welche den Streifen ungefähr auf die doppelte Länge ausdehnen. Nachdem man gewartet hat, bis die elastische Nachwirkung unmerklich geworden ist, beobachtet man den Stand des untern Endes des Streifens, etwa an einer daneben aufgestellten Papierscala, und lässt nun den Kautschuk von einem Gehülfen electriciren. Der Gehülfe hält zu diesem Zweck in jeder Hand einen isolirten Spitzenkamm, von denen der eine mit der positiven, der andere mit der negativen Electrode einer kräftigen Holtz'schen Maschine in leitender Verbindung steht; zwischen den parallel gehaltenen Kämmen hängt das Kautschukband, dasselbe wird aber nicht von den Spitzen berührt. Indem nun der Gehülfe etwa am obern Ende anfängt und allmählich mit beiden Kämmen herunterfährt, wird ein immer grösserer Theil des Kautschuks electricirt; dem entsprechend beobachtet man eine fortwährende Längenzunahme des Bandes, welche schliesslich, wenn der ganze Streifen electricirt ist, mehrere Centimeter beträgt. Da trockener Kautschuk ein guter Isolator ist, dauert diese Verlängerung längere Zeit. Dieselbe kann aber, wenigstens zum grössern Theil aufgehoben werden, indem man den Streifen entladet, was in ähnlicher Weise geschieht wie das Laden; nur müssen jetzt beide Kämmen zur Erde abgeleitet sein.

Auch Herr Quincke hat (1880) ähnliche Versuche veröffentlicht und glaubt aus denselben schliessen zu dürfen, dass die Elasticität der festen Körper durch electriche Kräfte geändert werde; ich halte eine solche Schlussfolgerung wiederum für sehr gewagt und habe nach einer Prüfung der Quincke'schen Versuche keine Veranlassung gefunden, diese Auffassung zu der meinigen zu machen; da ich jedoch befürchte, dass der vorliegende Aufsatz eine zu grosse Ausdehnung erhalten würde, so möchte ich die Mittheilung der Motive zu meinem ablehnenden Verhalten unterlassen.

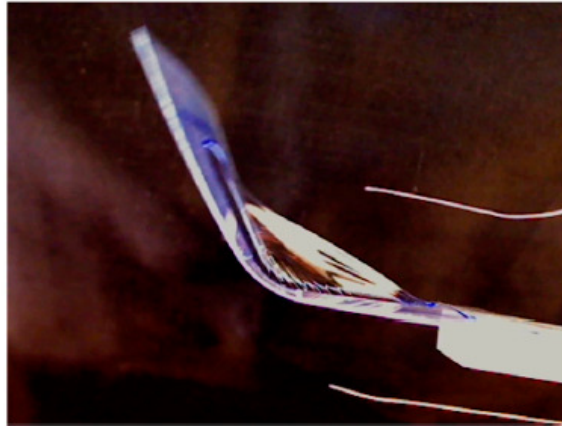
Giessen, September 1880.

Fig. 56. Extracts from Röntgen's original work in German.



Movie S1. Illustration of the reversibility of the large deformations of an elastomer surface with sprayed-on electrical charges.

[Movie S1 \(MPG\)](#)



Movie S2. Illustration of the operation of the electrode-free bending actuator.

[Movie S2 \(MPG\)](#)